Naval Surface Warfare Center

Carderock Division

West Bethesda, MD 20817-5700

NSWCCD-80-TR-2019/035 **November 2019**

Naval Architecture and Engineering Department

Technical Report

ASSESSMENT OF HYDRODYNAMIC AND STRUCTURAL ANALYSIS TOOLS FOR *R/V ATHENA* IN CALM WATER

by

Anne Fullerton, Jayson Geiser, Sarah Punzi, Jason Morin, Charles Weil, Don Walker, Evan Lee, Minyee Jiang, Van Lien, and Craig Merrill

NSWCCD

REPORT DOCUMENTATION PAGE

Form Approved
OMB No. 0704-0188

1. REPORT DATE *(DD-MM-YYYY)*	2. REPORT TYPE	3. DATES COVERED *(From - To)*
16-11-2019	Final	Aug 2014-Oct 2016

4. TITLE AND SUBTITLE

Assessment of Hydrodynamic and Structural Analysis Tools for R/V Athena in Calm Water

5a. CONTRACT NUMBER
N0001416WX00664

5b. GRANT NUMBER

5c. PROGRAM ELEMENT NUMBER

6. AUTHOR(S)
Anne Fullerton, Jayson Geiser, Sarah Punzi, Jason Morin, Charles Weil, Don Walker, Evan Lee, Minyee Jiang, Van Lien, and Craig Merrill

5d. PROJECT NUMBER

5e. TASK NUMBER

5f. WORK UNIT NUMBER
100001147500

7. PERFORMING ORGANIZATION NAME(S) AND ADDRESS(ES)
NAVSEA Carderock
Naval Surface Warfare Center
Carderock Division (Code 833)
9500 Macarthur Boulevard
West Bethesda, MD 20817-5700

8. PERFORMING ORGANIZATION REPORT NUMBER

NSWCCD-80-TR-2019/035

9. SPONSORING / MONITORING AGENCY NAME(S) AND ADDRESS(ES)
Dr. Robert Brizzolara, ONR 333
Office of Naval Research
875 North Randolph Street
Arlington, VA 22203-1995

10. SPONSOR/MONITOR'S ACRONYM(S)

11. SPONSOR/MONITOR'S REPORT NUMBER(S)

12. DISTRIBUTION / AVAILABILITY STATEMENT
DISTRIBUTION STATEMENT A. Approval for public release; distribution unlimited.

13. SUPPLEMENTARY NOTES

14. ABSTRACT
Current structural design methods for high-speed naval craft rely heavily on empiricism. Though these methods have been employed reliably for a number of years, it is likely that an unknown level of conservatism exists in the prediction of both global and local impact loads to ensure the vessel's structural design is robust.

15. SUBJECT TERMS
R/V Athena, resistance, semi-planing, CFD

16. SECURITY CLASSIFICATION OF:			17. LIMITATION OF ABSTRACT	18. NUMBER OF PAGES	19a. NAME OF RESPONSIBLE PERSON
a. REPORT	b. ABSTRACT	c. THIS PAGE			Alma Jacobson
Unclassified	Unclassified	Unclassified	None	vii+58	19b. TELEPHONE NUMBER *(include area code)* 757-492-4235

Standard Form 298 (Rev. 8-98)
Prescribed by ANSI Std. Z39.18

14. ABSTRACT (continued)

A better physical understanding of the dynamic response of high-speed craft in seas would allow for increased structural optimization. To support this understanding, a computational approach to predicting motions and loads was proposed. The publicly releasable hull form Naval Surface Warfare Center Carderock Division (NSWCCD) Model 5365 (*R/V Athena*) was chosen to facilitate public release of results to various computational teams. Model 5365 was tested in calm water, regular waves, and irregular waves. Initial comparisons of the experiments with STAR-CCM+ and CFDShip-Iowa predictions shows good agreement. Further comparisons with predictions should not be completed with this data set, as the forward tow point is cause for uncertainty in the experimental results.

Standard Form 298 (Rev. 8-98)

Prescribed by ANSI Std. Z39.18

CONTENTS

FIGURES

TABLES

ADMINISTRATIVE INFORMATION

The work described in this report was performed by the Naval Architecture and Engineering Department (Code 80) at the Naval Surface Warfare Center, Carderock Division (NSWCCD). The work was funded by the Office of Naval Research, Code 333, (N0001416WX00664) under the direction of Dr. Robert Brizzolara.

ACKNOWLEDGEMENTS

The authors would like to thank Dan Hayden, David Bochinski, Lawrence Snyder, and Christina Pico for their valuable assistance during model preparation and testing, as well as Dr. Thomas Fu for his valuable guidance during planning and testing. The authors would also like to thank Dr. Frederick Stern for providing his CFDShip-Iowa predictions.

SUMMARY

Current structural design methods for high-speed naval craft rely heavily on empiricism. Though these methods have been employed reliably for a number of years, it is likely that an unknown level of conservatism exists in the prediction of both global and local impact loads to ensure the vessel's structural design is robust. A better physical understanding of the dynamic response of high-speed craft in seas would allow for increased structural optimization. To support this understanding, a computational approach to predicting motions and loads was proposed. The publicly releasable hull form Naval Surface Warfare Center Carderock Division (NSWCCD) Model 5365 (*R/V Athena*) was chosen to facilitate public release of results to various computational teams. Model 5365 was tested in calm water, regular waves, and irregular waves. Initial comparisons of the experiments with STAR-CCM+ and CFDShip-Iowa predictions shows good agreement. Further comparisons with predictions should not be completed with this data set, as the forward tow point is cause for uncertainty in the experimental results.

INTRODUCTION

The physical test of Model 5365 was designed to provide a computational fluid dynamics (CFD) validation data set for semi-planing craft. The CFD predictions were evaluated in their ability to predict calm water performance, as well as motions and loads in regular and irregular waves. The measurements made during testing include:

1. Resistance, sinkage, and trim measurements for the model in calm water over a range of speeds.
2. Six degree-of-freedom (6-DOF) forces and moments acting on the model over a range of speeds and wave conditions.
3. Model motions and accelerations over a range of speeds and wave conditions.
4. Impact pressures over a range of locations on the model with the model at different speeds and wave conditions for model validation.

This report will focus on the calm water results; a subsequent report will present results from model testing in waves.

EXPERIMENTAL APPROACH

Facility Description

Measurements of the *Athena* model operating in calm water, regular, and irregular waves were performed in the Deep Water Basin at NSWCCD using towing Carriage 2. The basin is approximately 1886 feet long, 51 feet wide, and 22 feet deep. Carriage 2 has a maximum towing speed of 20 knots (33.8 ft/s). A pneumatic wavemaker is located at the east end of the basin, with a wave-absorbing beach at the west end.

Model Description

Model 5365 is an 8.25 scale model of the *R/V Athena*, shown in Figure 1. The *R/V Athena* is a converted PG-84 Asheville-class patrol gunboat, which is operated out of Naval Surface Warfare Center - Panama City Division as a high-speed research vessel. The model, built in 1979, was constructed out of wood and fiberglass. The model has been refurbished over its lifetime, and in 2002, it was measured using NSWCCD's laser tracker model measurement system. The detailed measurements of the model, shown in Figure 2 revealed an asymmetry in the hull in the region of the bow, on the starboard side of the model. This as-measured geometry is available from NSWCCD by request.

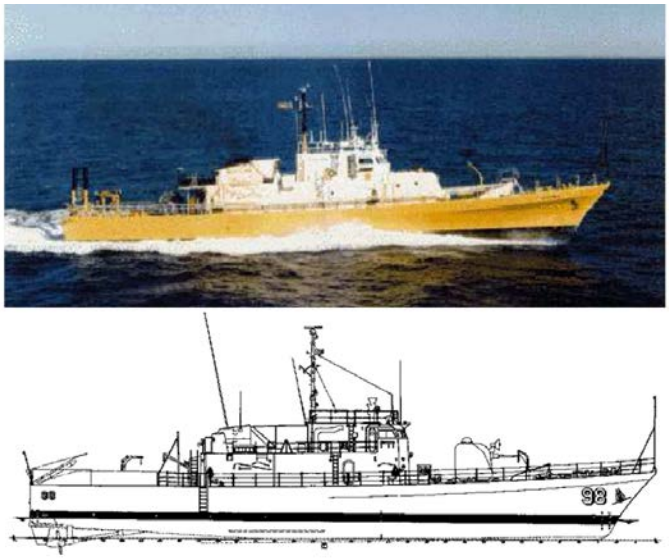

Figure 1. Full Scale *R/V Athena*

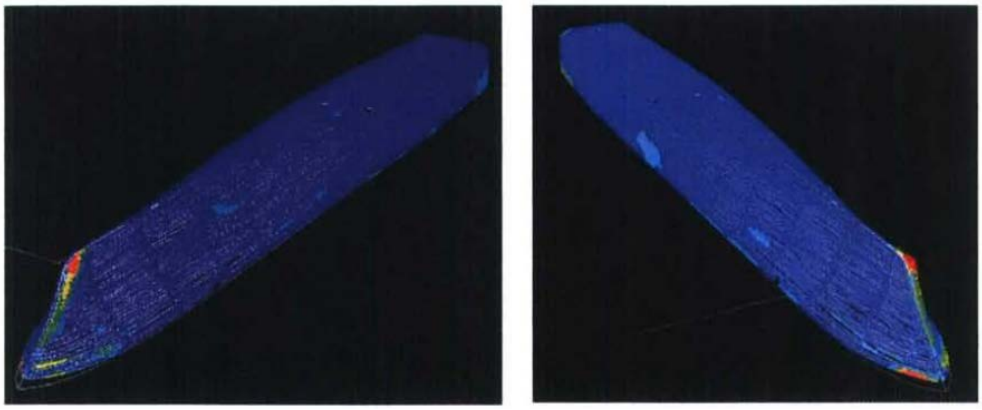

Figure 2. Laser Tracker Surface Measurements of Model 5635 (largest deviation is 0.04 inches as shown in red)

The model has been painted yellow on the port side to facilitate still and video photography, and black on starboard side, providing a non-reflective surface for previously conducted Q-Viz (a laser sheet quantitative flow visualization method) laser measurements, as shown in Figure 3. Turbulence stimulators were placed on the model along a line 2 inches aft of and parallel to the leading edge of the bow. The turbulence stimulators are acrylic cylinders, 1/8" high, with a diameter of 1/8". Table 1 shows the as-tested model scale particulars. The model was ballasted to the same waterline used during a 2006 test of the same model [1].

a) Port side. **b) Transom**

c) Bow region – Starboard Side

Figure 3. Images of Model 5365 showing the yellow and black paint scheme, waterlines, and station lines

Table 1. Model Particulars

Scale Ratio	8.25
Displacement	859.2 lbf
Length Between Perpendiculars (LBP)	18.67 ft
Maximum Beam	2.74 ft
Transom Beam	2.3 ft
Longitudinal Center of Tow Point (LTP, forward of AP)	14.186 ft
Longitudinal Center of Gravity (LCG, forward of AP)	7.92 ft
Vertical Center of Gravity (VCG , above baseline)	0.804 ft
Pitch Mass Moment of Inertia, I_y	21,073 (lb-ft2)
Pitch Radius of Gyration, k_y	4.953 ft
Draft at LCG (above baseline)*	0.609 ft
Length of the Waterline (LWL)	18.67 ft
Maximum Waterline Beam (BWL)	2.77 ft
Static Wetted Surface Area (S_o)	46.06 ft^2
Static Trim Angle from Baseline (+ bow up)*	0.2 deg

Notes: ABL is above baseline, * indicates that value was determined from hydrostatics and not measured directly

Test Conditions

The *Athena* model was tested in calm water, regular waves, and irregular waves at a variety of speeds. The testing conditions are listed in Table 2. Resistance testing consisted of the model operating at three different speeds with each speed held constant for just over 15 seconds. This allowed the team to collect 10 seconds of data at each speed before moving on to the next run. The basin was allowed to settle for 10 minutes between runs. In waves, a single length of the basin was collected for each run. After a regular wave run, the basin was allowed to settle for 25 minutes. In irregular waves, runs were conducted continuously for 30 minutes before the basin was given 25 minutes to settle. For this test, values of x are considered positive forward, and trim is positive bow up. Due to heave limitations imposed by the tow post, several larger wave conditions that were planned were not tested. These conditions were tested later in 2015 using a different tow post and different tow post location within the model. The calm water speeds were chosen to match resistance, sinkage, and trim curves from previous model tests [1]. The regular and irregular wave conditions were also based on previous tests, with additional conditions of interest as suggested by the CFD community investigating this model.

Table 2. *Athena* Test Conditions (Model Scale)

Speed (kts)	Fn	Wave Type	Wave Height/Hs (in)	Wave Period / Tp (s)
2.0	0.14	Calm		
3.1	0.22	Calm		
3.7	0.25	Calm		
4.2	0.29	Calm		
6.3	0.43	Calm		
9.0	0.62	Calm		
12.2	0.84	Calm		
3.7	0.25	Regular	9.1	1.9
6.3	0.43	Regular	9.1	1.9
9.0	0.62	Regular	9.1	1.9
3.7	0.25	Irregular	4.2	2.61
6.3	0.43	Irregular	4.2	2.61
9.0	0.62	Irregular	4.2	2.61

MEASUREMENT METHODS

Visualization

Digital video cameras with a frame rate of 30 fps were used to record the motion of the free surface from multiple views. The standard views included a profile view of the starboard side of the model and a bow quartering view on the starboard side. Video was digitized and backed up during testing.

Forces/Moments on the Ship Hull

The 6-DOF force measurements were acquired through two separate Kistler gauges mounted on the model. The main gauge was attached to the model above the tow point and measured the forces and moments during testing. There was an additional Kistler gauge mounted to a grasshopper mount at the stern of the model. The grasshopper mount is a balanced flexible arm that is designed to apply minimal vertical forces and is used to restrict yaw motions of the model. Because this additional mount can absorb some of the drag forces, the gauge is added in order to determine the total drag on the model. The Kistler gauges were manufactured at NSWCCD using four 3-axis Kistler force sensors (Type 9602A3211). Four sensors are used in each 6-DOF system to increase accuracy, effective range, and durability during testing. These sensors have an effective range of approximately ±500 lbf in the x and y direction, and ±900 lbf in z at 100 percent full-scale, but can be switched to operate at 10 percent of full-scale (±50 lbf in the x and y, and ±90 lbf in z). At full scale, the resolution is 0.45 lbf for x and y, and 0.41 lbf in z. The standard error for both scales is ±5 %. Conversion between voltage and force measurements was performed via a matrix calibration to remove crosstalk between the sensors. The calibration was conducted using a custom 6 DOF calibration rig fabricated at Carderock. A more detailed description of the Kistler gauges and calibration is included in Appendix A.

Ship Motion

A Kearfott KN-5050 inertial navigation system was the main motion package used on the test. The system included a ring laser gyro and is capable of using GPS or other position-based input. GPS correction was not used for this test. As mentioned previously, the Kearfott was rigidly mounted near the longitudinal center of gravity via a mounting platform. The Kearfott provided measurements of the craft's pitch, roll, and heading. The heading accuracy of the system is 0.44° RMS and the roll/pitch accuracy is 0.03° RMS. The Kearfott outputs data at 50 Hz.

Ship Trim/Pitch

Two string potentiometers (string pots) were used to measure vertical displacement of the model at the bow and the stern. The string pots used a UniMeasure model PA-50-004, which has a 50-inch range and a maximum error of ±0.125-inch. With knowledge of the initial string pot locations, the string pot measurements can be used to calculate sinkage/heave and trim/pitch. The string pots were placed as far apart as possible to increase the accuracy of the trim/pitch

calculation. The output voltages from the string pots were converted to inches of displacement following calibration at Carderock. Data was collected at 100 Hz during testing.

Eye screws were used to attach the strings to the model, near the bow and the stern, respectively. The forward string potentiometer location was 250.35 inches forward of the transom. The aft string potentiometer location was 0.35 inches forward of the transom.

Impact Pressure

Eighteen pressure gauges were mounted on the bottom of the model hull during testing, including fifteen NPI-19 series low pressure gauges and three EPX series miniature pressure transducers. Pressure data was collected at 6250 Hz during each run. These gauges were used to measure single point wave slamming pressures on the hull during the model tests in waves. The pressure gauge locations and sensor number are shown in Figure 4. Sensor numbers in boxes are NPI-19 gauges and sensor numbers in circles are EPX gauges. A three by three array of NPI-19 gauges with 1" spacing were mounted just aft of the highest pressure location determined from previous CFD simulations. Three sets of three pressure gauges, oriented in a vertical line, (two NPI-19 and one EPX) were mounted fore and aft of the nine gauge array to both increase the area of recoded pressure data and to serve as a benchmarking test to determine the most effective pressure gauge type and sealant for this testing.

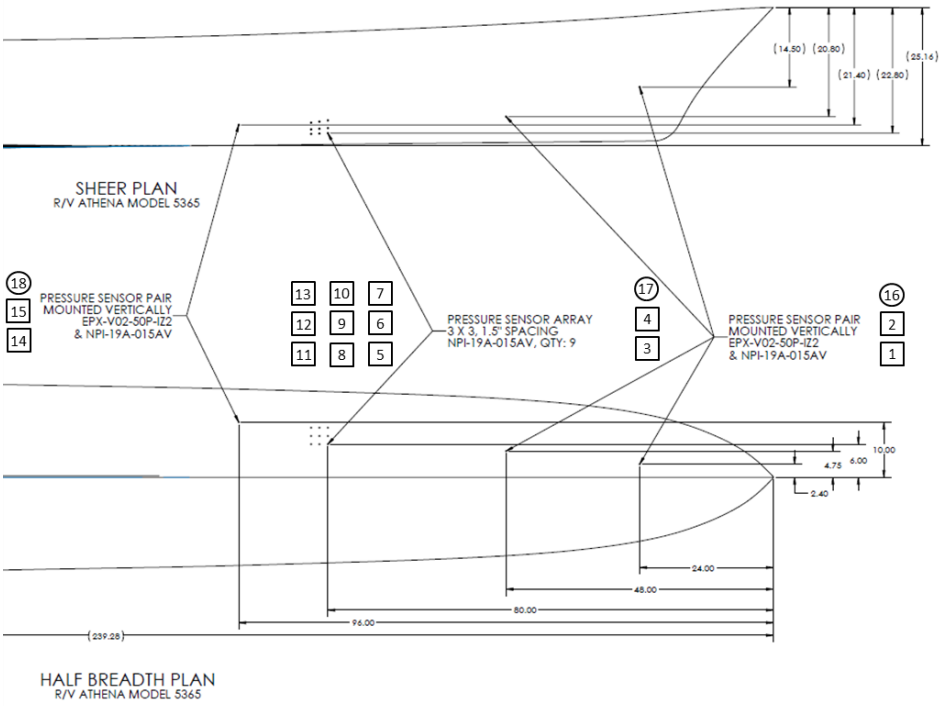

Figure 4. Pressure Gauge Locations and Sensor Number on *Athena* Model 5365

Wave Elevations

Senix ToughSonic Distance Sensors (model TSPC-15S-232) were used to measure wave height, both as a moving measurement on the carriage, and as a stationary measure of the wave field. A wave boom (truss section), cantilevered from the basin wall over the water, provided the

stationary structure from which the instrumentation was mounted. The wave boom extended 22.4 ft from the basin wall and contained three ultrasonic sensors. Three additional ultrasonic sensors were mounted forward, port, and starboard of the model on the carriage. The forward wave sensor was placed 18” from the foreword most point of the bow along the centerline of the ship. The port and starboard sensors were placed 2.4” from the foreword most point of the bow and 9” to each side of the hull centerline. These sensors provided near field wave data during the testing. The sensor data was collected at a frequency of 20 Hz.

Carriage Speed

Carriage 2 is equipped with an encoder that has been calibrated to output carriage speed. The speed readings were time-synced and recorded by the acquisition system. Encoder readings were validated with on-board carriage speedometers during testing.

Data Collection

Data was collected and time stamped using a LabVIEW based data acquisition program. The program display, as seen in Figure 5, was capable of displaying multiple variables on any of the four plots in real time. Rolling and total averages were also displayed alongside the data in real time. The program saved all data at 6250 Hz (the maximum sample rate of all instruments) into a text file for post-processing.

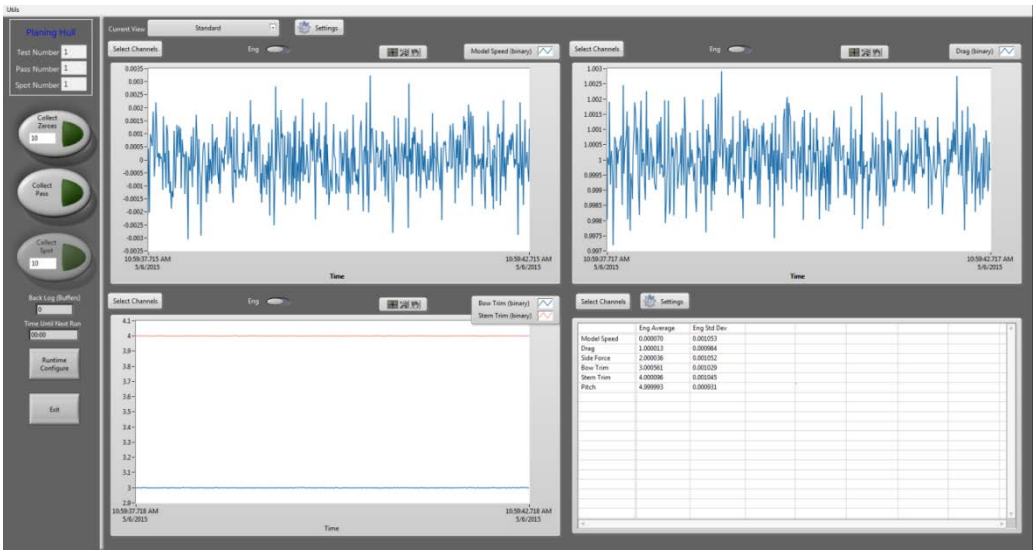

Figure 5. Screenshot of the LabVIEW Data Acquisition Program

RESULTS AND DISCUSSION

Calculations and Uncertainty

The model mass properties were measured using the process described in Appendix B. Table 3 shows the values and uncertainties for model mass properties relevant to calm water performance. Uncertainties were calculated via the methods prescribed in Reference 3, Chapter 4 and Appendix B. A detailed description of the uncertainty calculations is included in Appendix D.

Table 3. Uncertainty in Mass Properties

Description	Value	Uncertainty
Displacement	859.2 lbf	+/- 0.3 lbf
LCG	7.9 ft	+/- 0.008 ft
VCG	0.8 ft	+/- 0.04 ft

Resistance, sinkage and trim were calculated from the force and string pot data. The equation to calculate total resistance (R_t) for this experiment is:

$$R_t = F_{xfwd} + F_{xaft}\cos(\tau) + F_{zaft}\sin(\tau) \quad (1)$$

where F_{xfwd} = resistance measured at forward Kistler gauge, located under the tow post
F_{xaft} = longitudinal force measured at aft Kistler gauge, located under the grasshopper
F_{zaft} = vertical force measured at aft Kistler gauge, located under the grasshopper
τ = trim angle

The forward Kistler gauge is located above the model pivot point, so the direction is earth-fixed. The aft Kistler gauge is mounted to the model, so it needs to be corrected to earth-fixed resistance in the x-direction.

The equation to calculate trim angle from initial conditions is:

$$\tau = \text{asin}\left(\frac{\sigma_{FSP} - \sigma_{ASP}}{L_{SP}}\right) \quad (2)$$

where σ_{FSP} = sinkage at forward string potentiometer
σ_{ASP} = sinkage at aft string potentiometer

L_{FSP} = distance between string potentiometers

The values for these variables are shown in Table 4. The locations and variables are shown in the sketch in Figure 6 (initial condition) and Figure 7 (with trim). Values of x are positive forward, and trim is positive bow up. The solid circle marks the longitudinal center of gravity, while the open circle is the point where the tow post was connected to the model.

The data reduction equation for the sinkage at the tow point (σ_{TP}) from initial conditions is:

$$\sigma_{LCG} = \sigma_{ASP} + X_{TP}\left(\frac{\sigma_{FSP} - \sigma_{ASP}}{L_{SP}}\right) \tag{3}$$

where X_{TP} = x position of tow point (measured along the model from aft potentiometer)

The sinkage is measured from the initial static waterline; positive is up and negative is down.

Table 4. Values for Potentiometer Positions

X_{FSP} (measured from aft perpendicular)	236.75 in
X_{ASP} (measured from aft perpendicular)	0.35 in
L_{SP} (between potentiometers)	236.4 in
X_{LCG} (measured from aft potentiometer)	94.69 in
X_{TP} (measured from aft potentiometer)	169.88 in

Note: absolute positions are relative to aft potentiometer

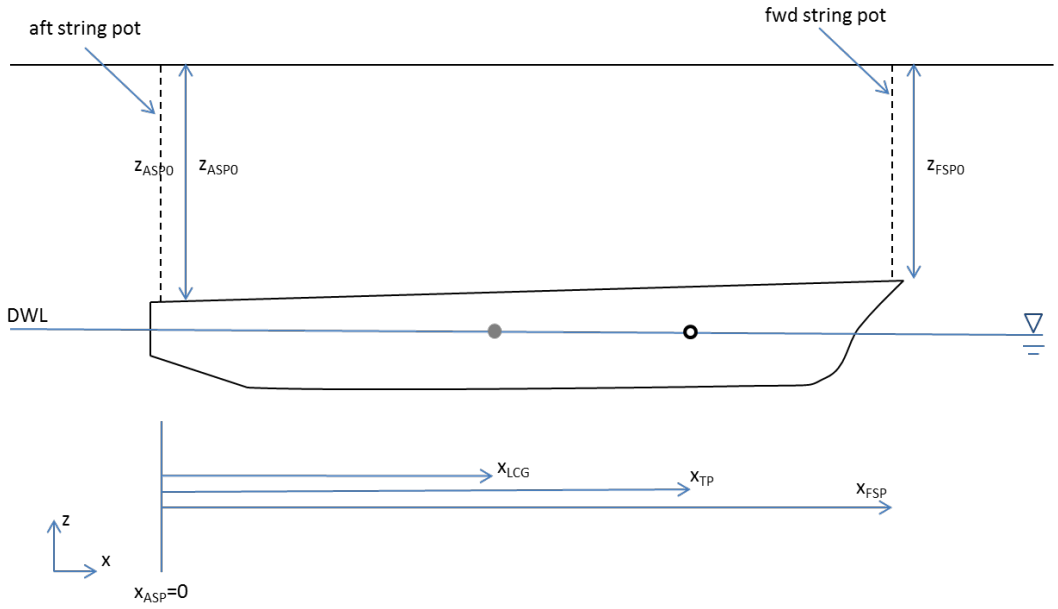

Figure 6. Sketch of *Athena* Model with String Pots in Initial Condition (not to scale; hull geometry is notional)

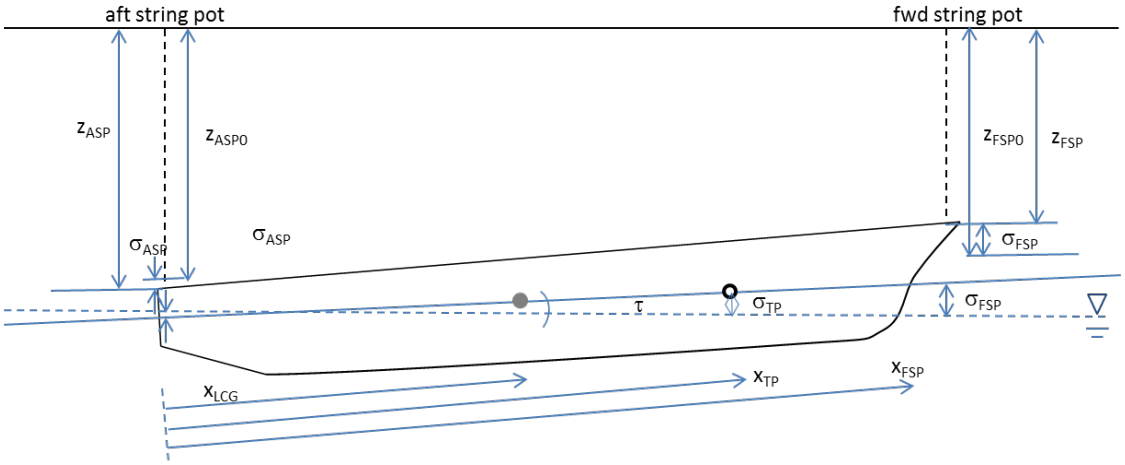

Figure 7. Sketch of *Athena* Model with String Pots with Trim (not to scale; hull geometry is notional)

Table 5, Table 6, and Table 7 summarize the results of the resistance, sinkage and trim calculations, along with their estimated bias (*B*), precision (*P*), and total (*U*) uncertainties (described in detail in Appendix D). Averages and uncertainties for carriage speed are also included (Table 8). The breakdown of bias uncertainties for each variable in the data reduction equations are also shown in the tables. The contribution of each uncertainty component is shown

either as a fraction of total bias uncertainty (for individual bias uncertainties) or as total uncertainty (for total bias and precision uncertainties).

The uncertainties are estimated at a 95% confidence interval, which means that there is 95% confidence that the true values lies within ±*U* of the reported value, *D* [2]. The ν value represents the degrees of freedom of the precision uncertainty calculation, which is the number of repeated runs less one. Each run was 10s long, and is a "spot" taken from a longer run down the tow basin. The basin was allowed to settle for 30 minutes between runs. Precision uncertainties are calculated using the end-to-end method described in Reference [2]. The bias error is the fixed or constant component of the total error and is referred to as systematic error. The precision (or random) error quantifies the repeatability of the measurement.

Table 5. Uncertainty and Values for Resistance Calculations

Resistance (lbf)														
	2.0 kts		*3.2 kts*		*3.6 kts*		*4.2 kts*		*6.2 kts*		*9.0 kts*		*12.2 kts*	
	value	*%B*	*value*	*%B*	*value*	*%B*	*value*	*%B*	*value*	*%B*	*value*	*%B*	*value*	*%B*
$B^2_{Fxfwd}\theta^2_{Fxfwd}$	1.96E-02	25%	1.96E-02	25%	1.96E-02	25%	1.96E-02	25%	1.96E-02	25%	1.96E-02	25%	1.96E-02	25%
$B^2_{Fxaft}\theta^2_{Fxaft}$	5.76E-02	75%	5.76E-02	75%	5.76E-02	75%	5.76E-02	75%	5.76E-02	75%	5.76E-02	75%	5.76E-02	75%
$B^2_{Fyaft}\theta^2_{Fyaft}$	2.85E-11	0%	1.92E-10	0%	2.80E-09	0%	3.39E-08	0%	6.29E-06	0%	3.19E-05	0%	2.84E-05	0%
$B^2_{\tau}\theta^2_{\tau}$	4.06E-10	0%	6.18E-10	0%	1.35E-10	0%	5.04E-09	0%	8.01E-11	0%	5.94E-09	0%	3.25E-08	0%
	value	*%U*	*value*	*%U*	*value*	*%U*	*value*	*%U*	*value*	*%U*	*value*	*%U*	*value*	*%U*
B_r	2.78E-01	11%	2.78E-01	18%	2.78E-01	14%	2.78E-01	17%	2.78E-01	13%	2.78E-01	19%	2.78E-01	5%
P_R	7.96E-01	89%	5.99E-01	82%	6.99E-01	86%	6.15E-01	83%	7.17E-01	87%	5.71E-01	81%	1.17E+00	95%
ν	8		9		9		9		9		9		9	
U_R	0.8		0.7		0.8		0.7		0.8		0.6		1.2	
D	3.0		8.4		10.0		14.5		30.6		55.8		86.1	
%U/D	28%		8%		7%		5%		3%		1%		1%	

Table 6. Uncertainty and Values for Trim Calculations

Trim (deg)														
	2.0 kts		*3.2 kts*		*3.6 kts*		*4.2 kts*		*6.2 kts*		*9.0 kts*		*12.2 kts*	
	value	*%B*	*value*	*%B*	*value*	*%B*	*value*	*%B*	*value*	*%B*	*value*	*%B*	*value*	*%B*
$B^2_{\sigma FSP}\theta^2_{\sigma FSP}$	2.86E-08	31%	2.86E-08	31%	2.86E-08	31%	2.86E-08	31%	2.86E-08	31%	2.86E-08	31%	2.86E-08	31%
$B^2_{\sigma ASP}\theta^2_{\sigma ASP}$	6.44E-08	69%	6.44E-08	69%	6.44E-08	69%	6.44E-08	69%	6.44E-08	69%	6.44E-08	69%	6.44E-08	69%
$B^2_{LSP}\theta^2_{LSP}$	9.06E-18	0%	6.10E-17	0%	8.91E-16	0%	1.08E-14	0%	2.00E-12	0%	1.01E-11	0%	9.02E-12	0%
	value	*%U*	*value*	*%U*	*value*	*%U*	*value*	*%U*	*value*	*%U*	*value*	*%U*	*value*	*%U*
B_{τ}	3.05E-04	3%	3.05E-04	9%	3.05E-04	2%	3.05E-04	2%	3.05E-04	0%	3.05E-04	0.0%	3.05E-04	0%
P_{τ}	1.74E-03	97%	2.82E-03	99%	2.09E-03	98%	2.00E-03	98%	5.42E-03	100%	1.38E-02	100%	1.65E-02	100%
ν	8		9		9		9		9		9		9	
U_{τ}	1.77E-03		2.83E-03		2.11E-03		2.03E-03		5.42E-03		1.38E-02		1.65E-02	
D	0.0		0.0		0.0		0.0		0.5		1.1		1.0	
%U/D	n/a		n/a		n/a		n/a		1%		1%		2%	

Table 7. Uncertainty and Values for Sinkage at Tow-Point Calculations

Sinkage LTP (in)														
	2.0 kts		*3.2 kts*		*3.6 kts*		*4.2 kts*		*6.2 kts*		*9.0 kts*		*12.2 kts*	
	value	*%B*	*value*	*%B*	*value*	*%B*	*value*	*%B*	*value*	*%B*	*value*	*%B*	*value*	*%B*
$B^2_{\sigma FSP}\theta^2_{\sigma FSP}$	8.26E-04	74%	8.26E-04	74%	8.26E-04	74%	8.26E-04	74%	8.26E-04	74%	8.26E-04	74%	8.26E-04	74%
$B^2_{\sigma ASP}\theta^2_{\sigma ASP}$	2.85E-04	26%	2.85E-04	26%	2.85E-04	26%	2.85E-04	26%	2.85E-04	26%	2.85E-04	26%	2.85E-04	26%
$B^2_{LSP}\theta^2_{LSP}$	2.61E-13	0%	1.76E-12	0%	2.57E-11	0%	3.12E-10	0%	5.77E-08	0%	2.93E-07	0%	2.60E-07	0%
	value	*%U*	*value*	*%U*	*value*	*%U*	*value*	*%U*	*value*	*%U*	*value*	*%U*	*value*	*%U*
B_σ	0.03	94%	0.03	94%	0.03	89%	0.03	96%	0.03	83%	0.03	22%	0.03	25%
P_σ	0.01	6%	0.01	6%	0.01	11%	0.01	4%	0.02	17%	0.06	78%	0.06	75%
ν	8		9		9		9		9		9		9	
U_σ	0.03		0.03		0.04		0.03		0.04		0.07		0.07	
D	0.0		-0.1		-0.2		-0.2		-0.1		0.7		1.0	
%U/D	n/a		26%		18%		17%		37%		10%		7%	

Table 8. Uncertainty and Values for Carriage Speed

	2.0 kts		*3.2 kts*		*3.6 kts*		*4.2 kts*		*6.2 kts*		*9.0 kts*		*12.2 kts*	
	value	*%U*	*value*	*%U*	*value*	*%U*	*value*	*%U*	*value*	*%U*	*value*	*%U*	*value*	*%U*
B_s	3.15E-04	0%	3.15E-04	2%	3.15E-04	2%	3.15E-04	1%	3.15E-04	1%	3.15E-04	0%	3.15E-04	0%
P_s	0.01	100%	0.00	98%	0.00	98%	0.00	99%	0.00	99%	0.01	100%	0.01	100%
ν	8		9		9		9		9		9		9	
U_s	0.01	100%	0.00	100%	0.00	100%	0.00	100%	0.00	100%	0.01	100%	0.01	100%
D	2.1		3.1		3.7		4.2		6.3		9.0		12.2	
%U/D	0.6%		0.1%		0.1%		0.1%		0.0%		0.1%		0.1%	

An additional measurement of trim was made using the Kearfott sensor, and a comparison between the two trim measurements was made. The trend between the two sensors is the same, but there appears to be a constant offset of 0.2 degrees between them. Though the assumption was that the initial trim of the model was zero because it was ballasted to the waterline, it was later found that the model waterline was marked incorrectly. There is approximately 0.6" difference in the waterline between the forward and aft perpendicular, resulting in an initial static trim of 0.2 degrees. Additionally, the Kearfott was installed with a slight angle relative to the baseline. This installation angle accounts for the additional static offset between the measurements and was removed during data reduction.

The precision (random) uncertainty accounts for nearly all of the uncertainty in the calculations for resistance and trim, and for sinkage at the higher speeds. The larger random uncertainties appear to be attributed to two factors: the unsteadiness over the run (the run length may not have been long enough for the model to settle); and, the 30 minute settling time between runs may have been insufficient.

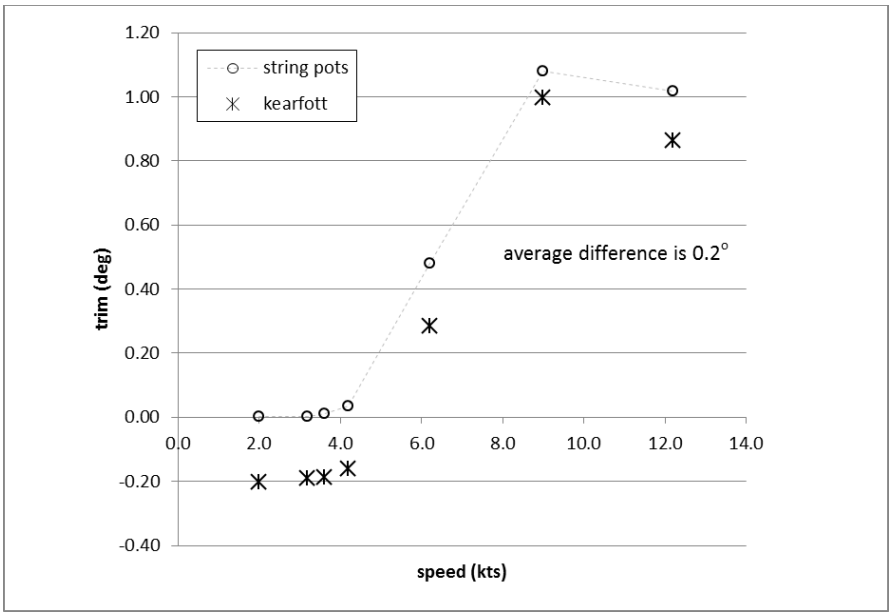

Figure 8. Trim Comparison of String Pot-Calculation and Kearfott Measurement

Unsteadiness in the run is shown in Figure 9, a plot of the raw x-force from the forward Kistler gauge, and the raw forward string pot displacement for a 30s 9 knot run (most runs were only 10s long as described above). The x-force plot shows constant oscillations in the force that continue over the course of the run. The range of force values is about 10 lbf, though they appear to oscillate around a consistent mean. The frequency of the oscillations is about 3 Hz; this is likely due to an excitation of the model whose natural frequency is about 1 Hz. The string pot shows a constant increase to the end of the 30s run, where it appears to settle out. Figure 10 shows another 9 knot run, but this run is the second run of the day. The force plot shows that there are again oscillations at about 3 Hz, but here the range is about 20 lbf (as opposed to 10 lbf.) Oscillations are also present in the string pot, but note that the value starts close to the stop value at the end of the run in Figure 9.

Figure 11, Figure 12, and Figure 13 show the mean (point) and standard deviation (error bars) for resistance, sinkage, and trim for the four 10s spots in Figure 9 and Figure 10, as well as one additional spot. The first three spots (111, 112, and 113) are from the first run of the day, and the last two spots (114 and 115) are from the second run of the day. These figures show the increase in standard deviation after the first run of the day (which includes the first three points, or spots). There is also an increase in the mean after the first run of the day. This trend suggests that more than 30 minutes is needed for the tank to settle between runs for this basin and test configuration.

For future testing, a sensitivity analysis should be performed to determine an appropriate balance between standard deviation and settling time. Another option is to reduce the duration of the wave reflections in the basin by increasing the amount of wave absorption on the basin walls using swim lane divers. Along with the longer settling time, a longer run (greater than 10 seconds) should also be used, due to the time it takes for the sinkage/trim to stabilize, as shown in Figure 9. It is recommended to maintain the same speed for each run down the tank to obtain longer data records.

Table 9 shows the potential advantage of this type of testing. The means and standard deviations were calculated for all of the 9 knot runs, and then calculated again after separating out the runs with settling times of less than and greater than 30 minutes. With a settling time of one hour or more, there is a reduction in resistance standard deviation by a factor of about 18, and a reduction in trim standard deviation by a factor of about four. Sinkage standard deviation is not reduced; the reason for this appears to be that the run length was not long enough, although basin seiching may also contribute to the data scatter. An investigation of other runs suggests that a one-hour settling time should be sufficient (i.e. a run performed after a lunch break yielded similar standard deviations to the first run of the day).

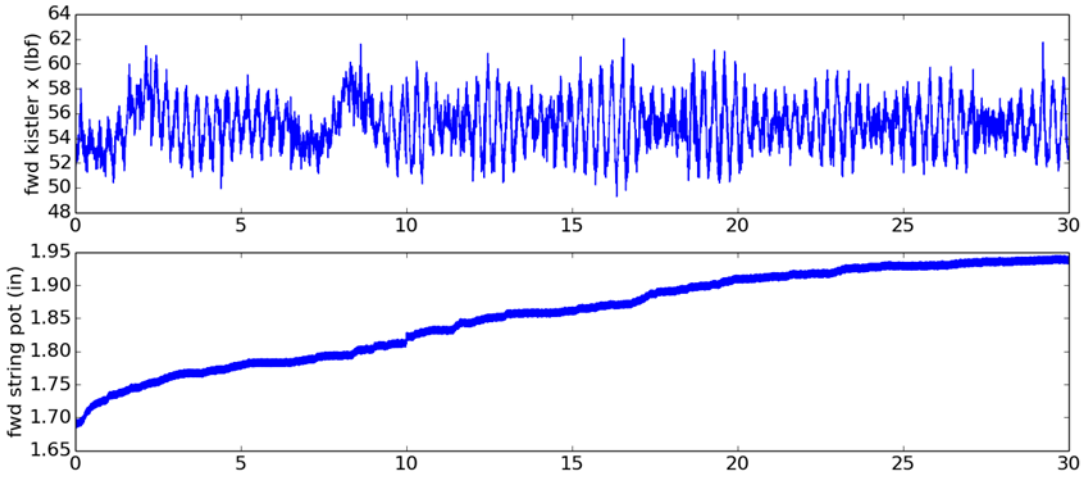

Figure 9. Plot of Raw String-Pot Output and Forward x-Force for 9 Knot Run.

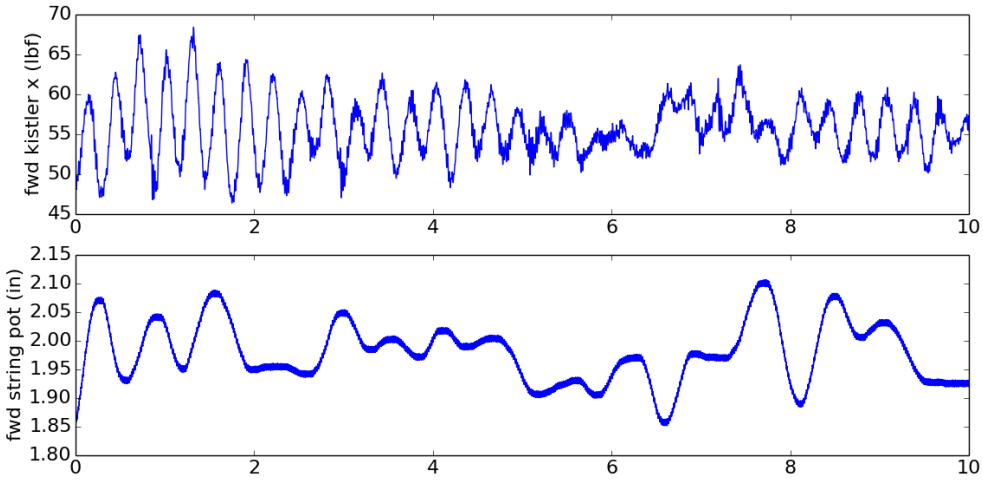

Figure 10. Plot of Raw String-Pot Output and Forward x-Force for 9 Knot Run

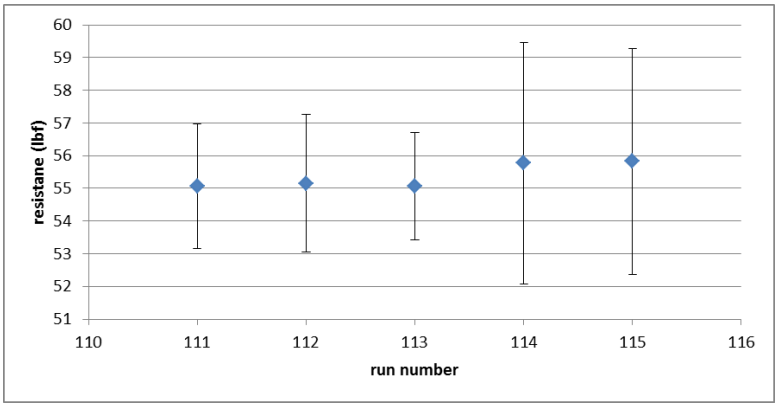

Figure 11. Mean and Standard Deviation of Resistance for Five 9 Knot Runs

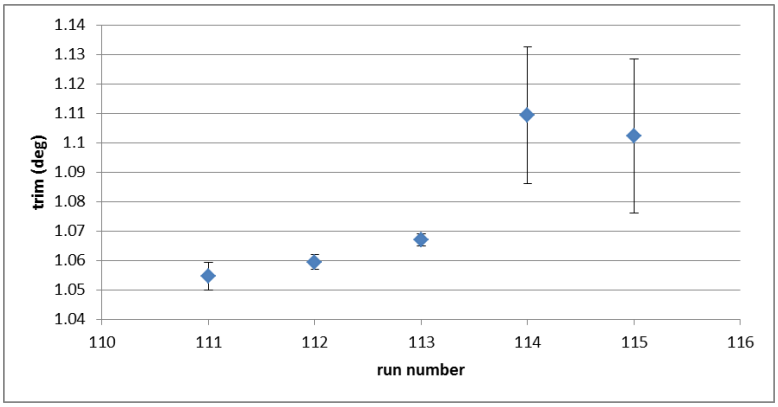

Figure 12. Mean and Standard Deviation of Trim for Five 9 Knot Runs

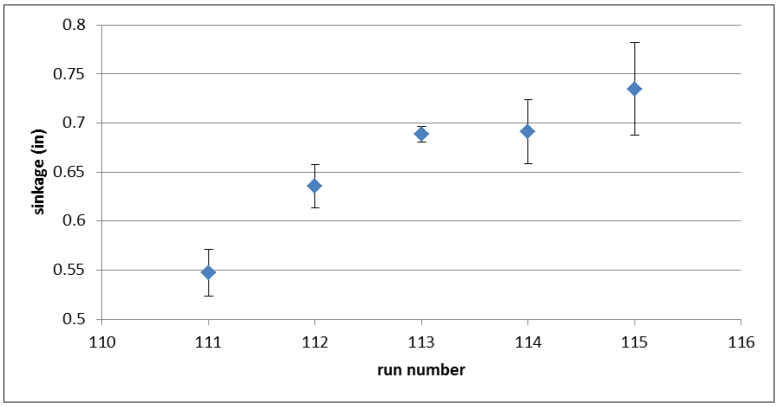

Figure 13. Mean and Standard Deviation of Sinkage for Five 9 Knot Runs

Table 9. Mean and Standard Deviation of 9 Knot Runs for Various Settling Times

	All Runs		*30 min settling*		*>30 min settling*	
9 kts	*mean*	*SD*	*mean*	*SD*	*mean*	*SD*
R_T *(lbf)*	55.8	0.798	56.3	0.630	55.0	0.045
τ *(deg)*	1.1	0.019	1.1	0.014	1.1	0.005
σ_{TP} *(in)*	0.7	0.088	0.8	0.052	0.7	0.085

Comparisons with 2007 Experiment

Table 10 shows the comparison between the data from this test and a similar test performed in 2007 [1]. Sinkage at the forward and aft perpendicular was reported for the 2007 test; these measurements were used to compute trim and sinkage at the tow post location for the 2014 test to enable comparisons of the results. Figure 15, Figure 16, and Figure 17 show comparisons of the data from Table 10 on plots of resistance, trim, and sinkage, respectively. The 2007 experiment collected data at a larger range of speeds, so there are additional points plotted to show trends.

The correlation (r^2), root-mean-square (*RMS*) error, and average angle measure (*AAM*) values were calculated between the data sets in order to quantify how well the data sets compare. Correlation between the data sets is a good description of how well the trends are matched, however the absolute values from one data set can be offset from the other data set and still have good values of correlation (close to 1). The *RMS* error yields an estimate of the average difference between the two data sets. *AAM* is a measure of the goodness of fit between two sets of variables, based on the average angle between the two data sets weighted by the distance from the origin (defined in Eq. 4 [4] and Figure 14). *AAM* yields a value between –1 and 1. A value of 1 corresponds to perfect magnitude and phase correlation, -1 implies perfect magnitude correlation but 180° out of phase and zero indicates no magnitude or phase correlation.

The correlation between the two data sets is very good. There is a small RMS error between the two data sets for resistance and sinkage, but it is less than the average uncertainty for these variables. The *AAM* values for these two data sets are very good for resistance, sinkage and trim. The resistance plot shows that the 2007 resistance values are just outside the uncertainty estimates for the 2014 test. Uncertainty values are not available for the 2007 data, but it is assumed that the range is similar to this test given that the model, conditions and instrumentation were the same. This assumption would mean that the uncertainty bands around the two sets of resistance data would overlap, showing relatively good agreement between the two data sets. The plots for trim and sinkage follow accordingly. The agreement between these two data sets demonstrates the intra-lab repeatability of this test, though it should be noted that the larger precision uncertainties improve the ability for the two datasets to agree. It would be desirable to decrease the precision uncertainties during testing, through longer runs and settling times as discussed above.

$$AAM = 1 - \frac{4}{\pi}\left[\frac{\sum_{n=1}^{N} D(n)\,|\,\alpha(n)\,|}{\sum_{n=1}^{N} D(n)}\right] \tag{4}$$

where:

$$\alpha_j(n) = \cos^{-1}\left[\frac{|\,m_j(n) + p_j(n)\,|}{\sqrt{2}\;D_j(n)}\right] \tag{5}$$

and:

$$D_j(n) = \sqrt{m_j^2(n) + p_j^2(n)} \tag{6}$$

where $m_j(n)$ is the point from one data set, and $p_j(n)$ is a point from another data set.

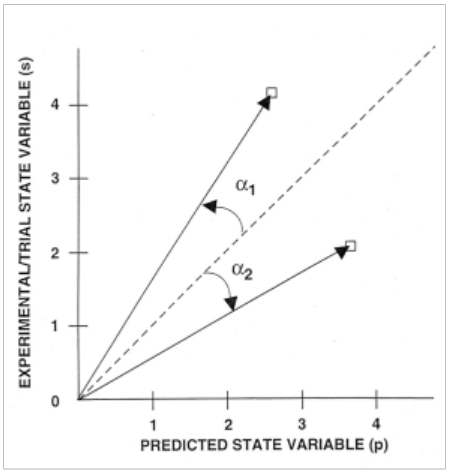

Figure 14. Definition of AAM Comparison between Two Data Sets

Table 10. Comparison of 2007 and 2014 Experimental Results

U (kts)	*R_T (lbf)*		*τ (deg)*		*σ_{TP} (in)*	
	2014	*2007*	*2014*	*2007*	*2014*	*2007*
2.1	3.0	2.8	0.0	0.0	0.0	-0.1
3.1	8.4	7	0.0	0.0	-0.1	-0.2
3.7	10.0	9.8	0.0	0.0	-0.2	-0.2
4.2	14.5	13	0.0	0.0	-0.3	-0.3
6.3	30.6	31	0.5	0.5	-0.1	-0.1
9.0	55.8	56	1.1	1.2	0.7	1.0
12.2	86.1	83	1.0	1.1	1.0	1.2
r^2	1.00		1.00		1.00	
RMS	0.06		0.00		0.03	
AAM	0.98		0.94		0.86	

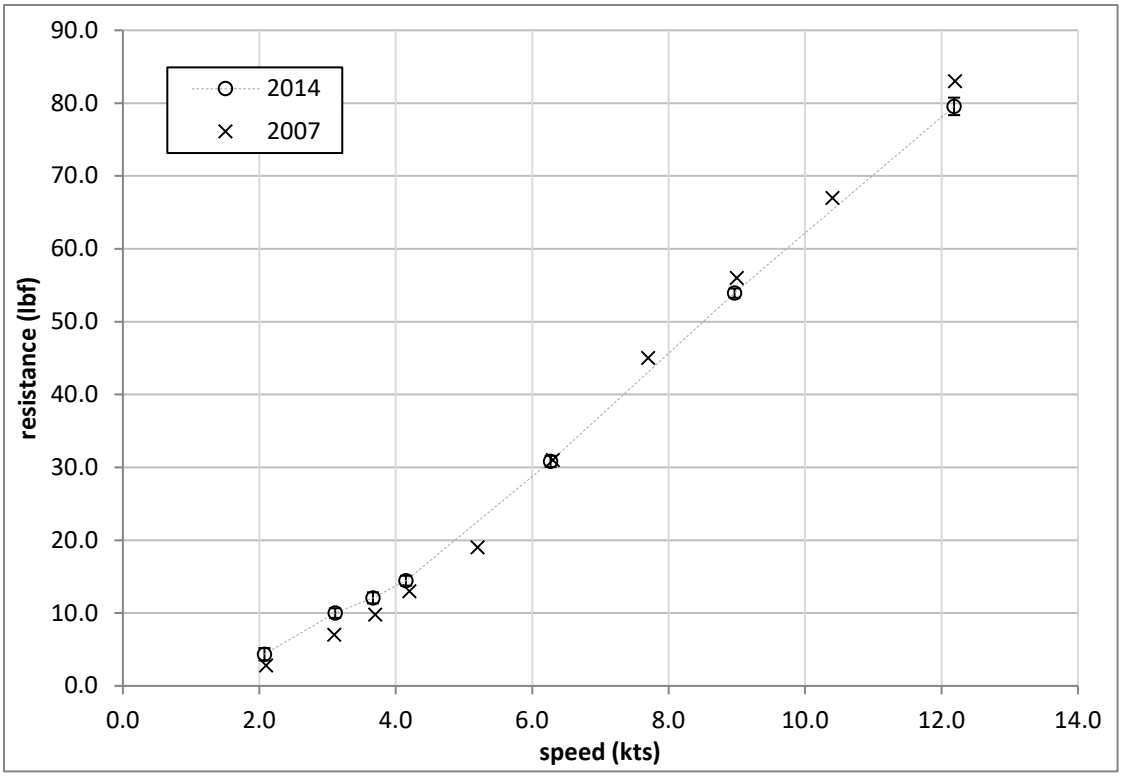

Figure 15. Resistance Comparison between 2007 and 2014 *Athena* Model Tests

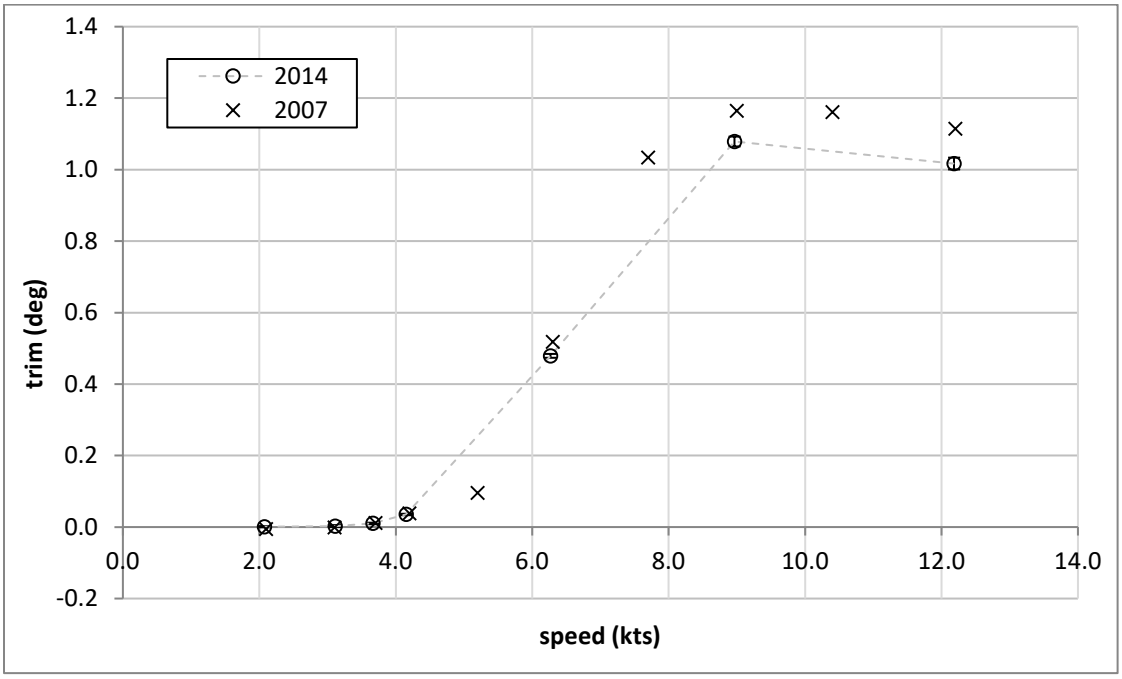

Figure 16. Trim Comparison between 2007 and 2014 *Athena* Model Tests

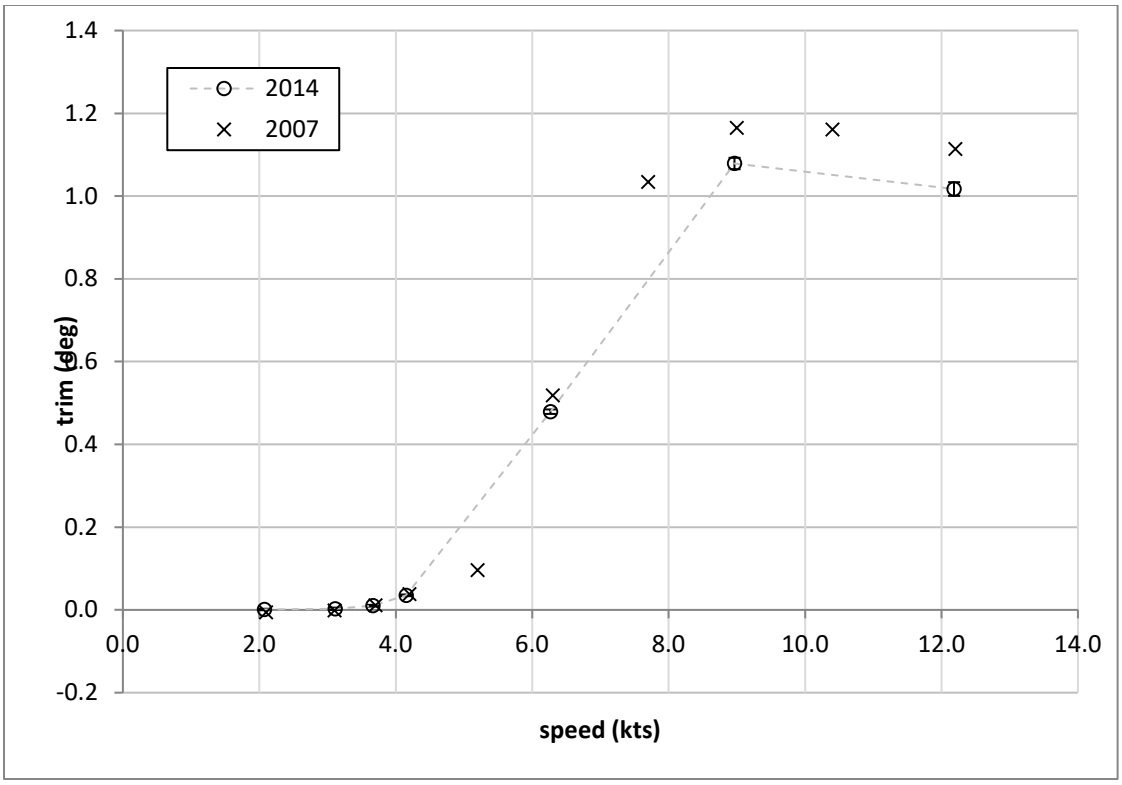

Figure 17. Sinkage (at TP) Comparison between 2007 and 2014 *Athena* Model Tests

Comparisons with CFD

Predictions of the *Athena* model in calm water were performed using three different computational codes: CFDShip-Iowa, STAR-CCM+ and the Large Amplitude Motions Program (LAMP). The single-phase level-set solver CFDShip-Iowa V4.5 is an incompressible Unsteady Reynolds-Averaged Navier-Stokes (URANS) solver designed for ship hydrodynamics.

STAR-CCM+ is a Reynolds-Averaged Navier Stokes (RANS) solver that is capable of modeling irregular seas, as well as regular sinusoidal waves. It has a robust meshing tool that needs little user interaction, and a volume of fluid (VOF) solver, which is useful for wave impact and fluid-structure interactions. The VOF approach assumes that the grid cells near the free surface are filled with both air and water, and within each grid cell, the VOF, pressure, velocity and gravitational force acting on the fluid is calculated. The ocean waves and the free surface are tracked by using the VOF values in the domain. This code has been applied in several past efforts concerning planing craft and surface ships. Using STAR-CCM+, Jiang et al. [4], predicted wave impact loads on a flat plate and simulated wave impact on a submarine with an external payload. STAR-CCM+ was also recently used to reasonably predict impact pressures for a wedge drop test at NSWCCD [5].

LAMP is a time domain simulation model developed for predicting the motions and loads of a ship operating in extreme sea conditions. LAMP uses a time-stepping approach in which all forces and moments acting on the ship are computed at each time step and the 6-DOF equations of motions are integrated in the time-domain using a 4th-order Runge-Kutta algorithm. In

addition to motions, LAMP also computes main hull-girder loads using a rigid or elastic beam model and includes an interface for developing Finite-Element load data sets from the 3D pressure distribution [6].

Table 11, Table 12, and Table 13 show the experimental and computational values for resistance, trim, and sinkage. In general, the r^2 and *AAM* between the experimental values and the predictions made by CFDShip-Iowa and STAR-CCM+ are very good (close to 1). The *RMS* errors between the experiment and the CFDShip-Iowa and STAR-CCM+ predictions are on the order of the experimental uncertainty. This is not the case for the LAMP predictions. LAMP tends to over predict resistance and sinkage, and under predict trim. The correlations are good for resistance and sinkage, which means the trends are similar, but the *AAM* values are not good, which means that the values are off in phase and magnitude. These results are not surprising given that LAMP is designed for ship motion predictions in waves, not in calm water. The poor performance in calm water does not necessarily indicate that LAMP will not be a good predictor of motions in waves.

Figure 18 is a comparison of the experimental data with the computational predictions of resistance; the error bars plotted on the experimental data indicate the experimental uncertainty. Since there is a large offset with the LAMP predictions, a plot without LAMP is shown in Figure 19 to better examine the performance of CFDShip-Iowa and STAR-CCM+. This plot shows the good agreement between the predictions and experimental measurements from this test; the predictions are within the uncertainty limits at the lower speeds and fall outside of the uncertainty limits at the high speeds. This visual agreement supports the r^2 and *AAM* values reported in Table 11.

Figure 20 is a comparison of the experimental data with the computational predictions of trim; the error bars plotted on the experimental data indicate the experimental uncertainty. Again, there is a large offset from the data for the LAMP predictions. Although the correlation and *AAM* values are close to 1.0 for trim, the predictions are outside the uncertainty estimates for the experimental data. Because the trim angles are small, the absolute difference between the experimental and predicted values is very small; they are outside the uncertainty bands by less than 0.2 degrees.

Figure 21 is a comparison of the experimental data with the computational predictions for sinkage; the error bars plotted on the experimental data indicate the experimental uncertainty. Since there is a large offset with the LAMP predictions, a plot without LAMP is shown in Figure 22 to better examine the performance of CFDShip-Iowa and STAR-CCM+. This plot shows the good agreement between the predictions and experimental measurements from this test; the predicted values fall outside the uncertainty limits. There is increased variability at the lower displacement speeds where the sinkage is near zero. This visual agreement supports the r^2 and *AAM* values reported in Table 11.

Table 11. Experimental and Computational Values for Resistance

V (kts)	R(lbf)			
	exp	*CFDShip-Iowa*	*StarCCM+*	*LAMP*
2.1	3.0	4.3	3.4	5.7
3.1	8.4	10.0	8.3	11.7
3.7	10.0	12.1	10.4	15.7
4.2	14.5	14.4	13.0	20.3
6.3	30.6	30.8	29.4	48.7
9.0	55.8	53.9	52.4	112.0
12.2	86.1	79.6	79.0	199.2
r^2		1.00	1.00	0.99
AAM		0.96	0.96	0.59
RMS (lbf)		2.8	3.0	48.4

Table 12. Experimental and Computational Values for Trim

V (kts)	trim (deg)			
	exp	*CFDShip-Iowa*	*StarCCM+*	*LAMP*
2.1	0.0	0.0	0.0	0.0
3.1	0.0	0.1	0.0	0.0
3.7	0.0	0.1	0.0	0.0
4.2	0.0	0.1	0.0	-0.1
6.3	0.5	0.5	0.5	0.1
9.0	1.1	1.0	0.9	0.7
12.2	1.0	0.9	0.9	0.6
r^2		1.00	1.00	0.94
AAM		0.93	0.91	0.58
RMS (deg)		0.0	0.1	0.3

Table 13. Experimental and Computational Values for Sinkage at Tow Post

V (kts)	sinkage at TP (in)			
	exp	*CFDShip-Iowa*	*StarCCM+*	*LAMP*
2.1	0.01	-0.04	-0.08	2.15
3.1	-0.13	-0.08	-0.14	2.14
3.7	-0.19	-0.13	-0.05	2.12
4.2	-0.28	-0.16	-0.16	2.10
6.3	-0.10	-0.05	-0.10	1.95
9.0	0.73	0.90	0.67	2.12
12.2	1.02	1.15	0.93	2.70
r^2		0.99	0.98	0.56
AAM		0.83	0.86	0.09
RMS (in)		0.1	0.1	2.1

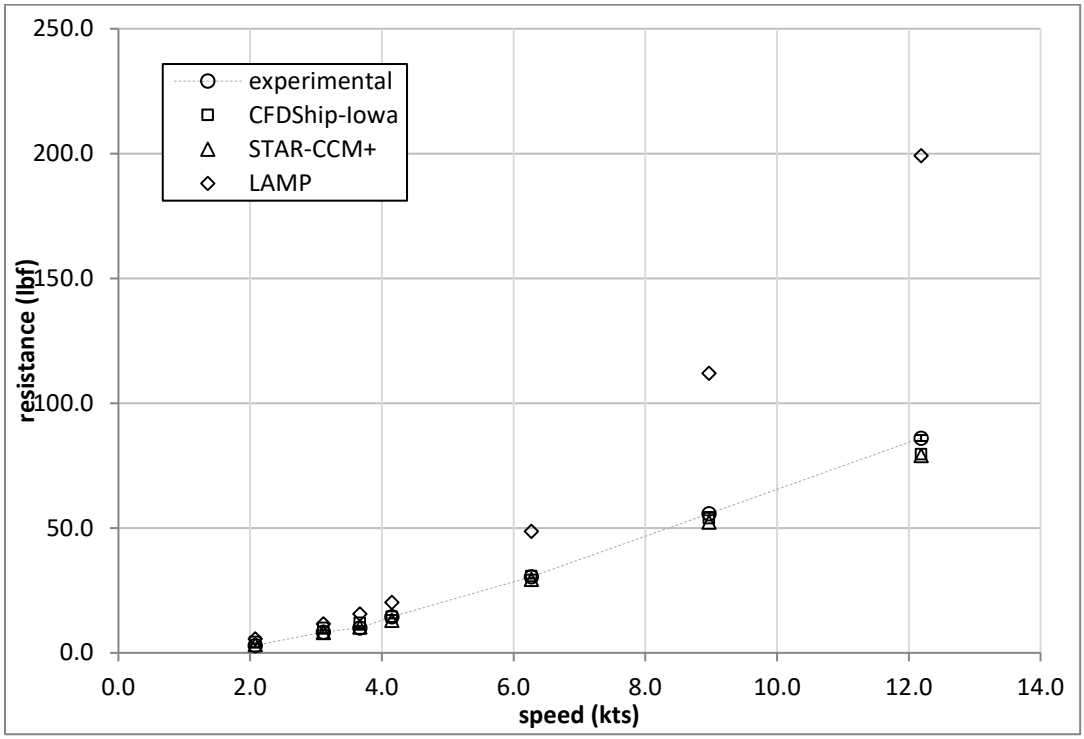

Figure 18. Experimental Resistance Comparisons with CFD Predictions

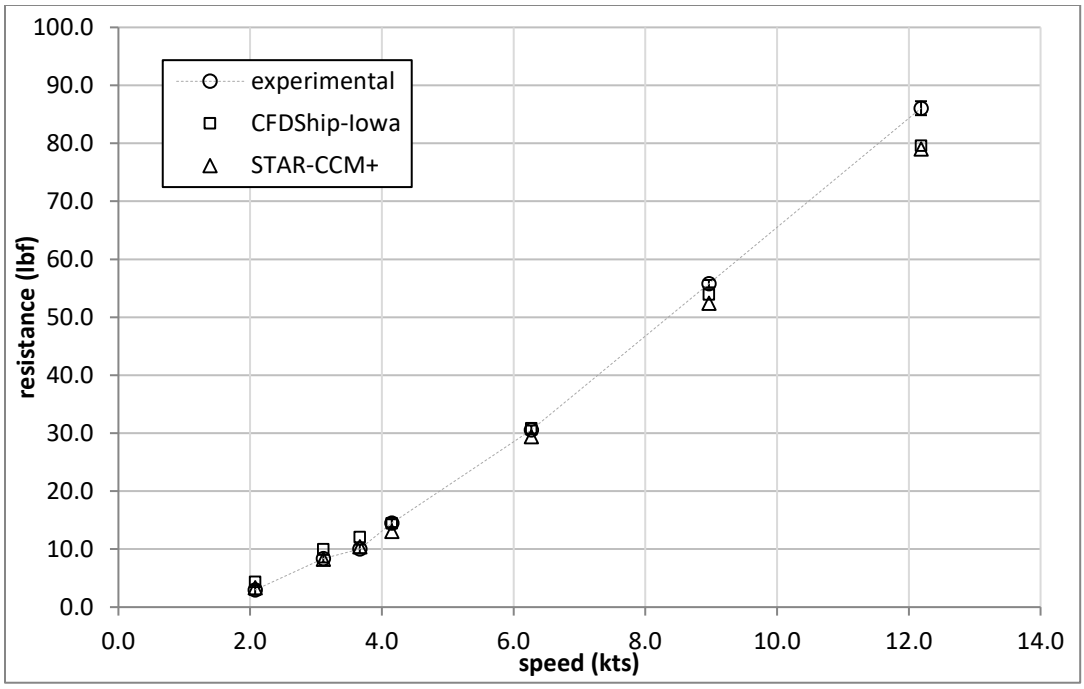

Figure 19. Experimental Resistance Comparisons with CFD Predictions (without LAMP)

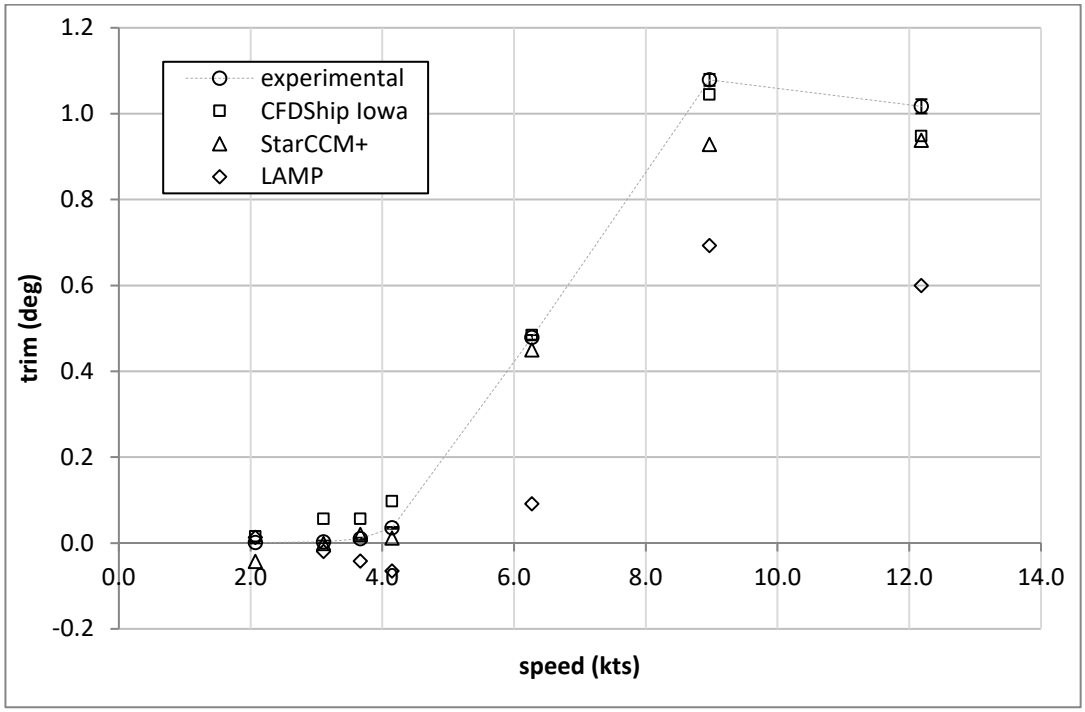

Figure 20. Experimental Trim Comparisons with CFD Predictions

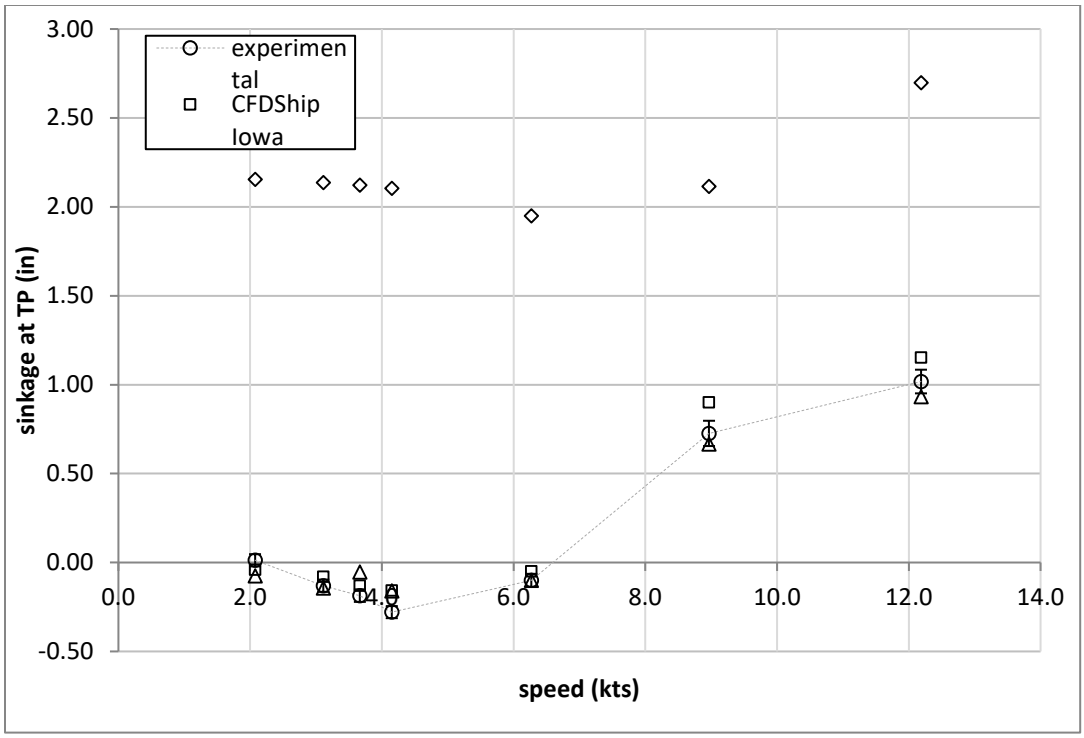

Figure 21. Experimental Sinkage (at TP) Comparisons with CFD Predictions

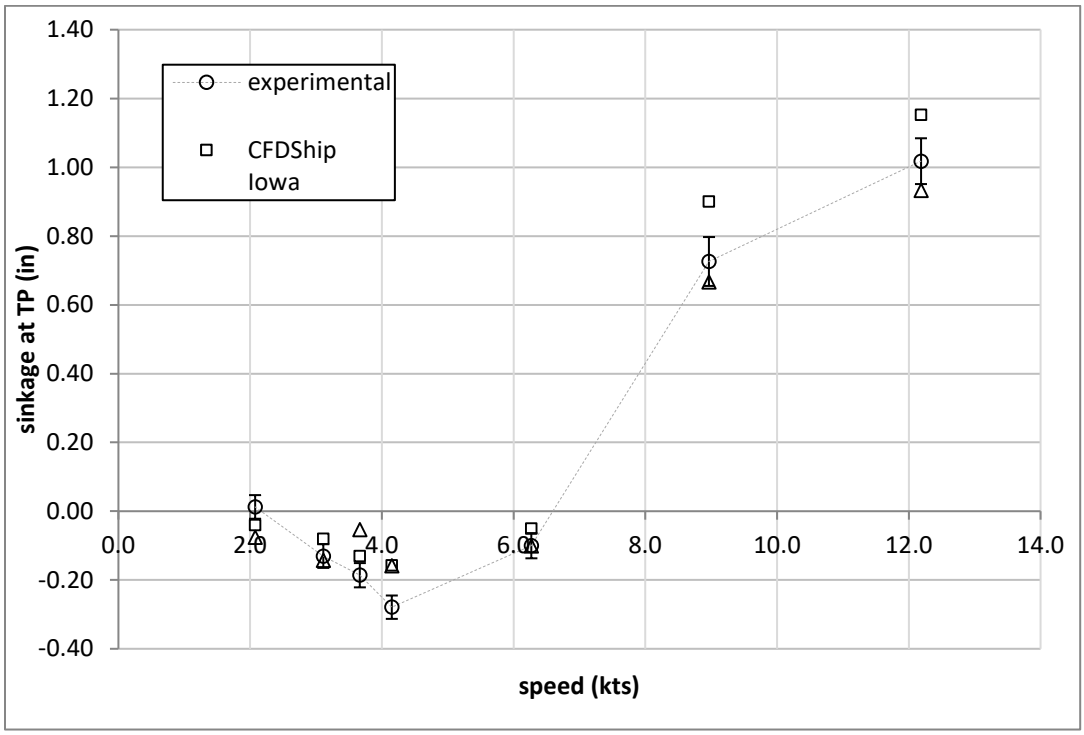

Figure 22. Experimental Sinkage (at TP) Comparisons with CFD Predictions (without LAMP)

CONCLUSIONS

A detailed uncertainty analysis was performed on the data collected for this test. This analysis demonstrated that the largest portion of total uncertainty comes from the precision uncertainties; longer test runs and longer settling times are proposed to overcome these issues for future testing. For future testing, a sensitivity analysis should also be performed to determine an appropriate balance between standard deviation and settling time. An additional issue that was discovered after testing was that there is approximately 0.6” difference in the waterline between the forward and aft perpendicular on the *Athena* model, resulting in an initial static trim of 0.2 degrees.

A comparison of this data to the data from the 2007 test shows relatively good agreement in resistance, sinkage, and trim, which demonstrates the intra-lab repeatability of the test (noting that the uncertainty bands are not negligible). This comparison gives confidence in using this dataset as a ground-truth comparison for CFD simulations. Comparisons of the computational predictions by STAR-CCM+ and CFDShip-Iowa show good agreement for resistance and sinkage, as demonstrated by the values of *AAM* and correlation. The resistance predictions are within the uncertainty limits at the lower speeds and fall outside of the uncertainty limits at the higher speeds. The predicted sinkage values fall outside the uncertainty limits. At the lower speeds, however, the sinkage is close to zero and the differences are very small. Comparisons of predictions of experimental trim with STAR-CCM+ and CFDShip Iowa show good agreement through the correlation and *AAM*, but the predicted values fall outside the uncertainty range of the experimental values. However, the absolute values of these differences are small, less than 0.2 degrees. Overall, the results from LAMP predictions do not agree with the experimental values; LAMP over predicts resistance and sinkage, and under predicts trim. The agreement between the STAR-CCM+ and CFDShip-Iowa predictions and experiments is encouraging. The good agreement supports the continuation of using these codes to predict performance in waves for future work. The poor agreement for LAMP in calm water does not necessarily indicate that it should not be used for predictions in waves; LAMP was not designed to predict performance in calm water.

In order to test Model 5365 in larger wave conditions in the future, it is necessary to refurbish the model as well as build a more robust tow-post with a larger heave range. By moving the tow location of the model to the CG and adding $\pm$ 3 inches of travel to the tow post, the model will be free to pitch and heave in significantly larger sea states than those used in this experiment, allowing for a wider variety of experimental conditions to compare with CFD results.

REFERENCES

[1] Ratcliffe, T., Fullerton, A., Rice, J., Walker, D., Russell, L., and Fu, T.C., “A Compendium of Resistance, Sinkage and Trim, and Longitudinal Wave Cut Measurements Obtained on Model 5365,” Naval Surface Warfare Center, Carderock Division, Hydromechanics Directorate R&D Report, NSWCCD-50-TR-2007/002, September 2007.

[2] Coleman, H. and W. G. Steele. *Experimentation and Uncertainty Analysis for Engineers*, Second Edition, John Wiley and Sons, New York, 1999.

[3] Ammeen, E. “Evaluation of Correlation Measures,” CRDKNSWC-HD-0406, Hydromechanics Directorate Research and Development Report, March 1994.

[4] Jiang, M., Lee, J., and Drazen, D. A., "CFD Modeling of a Submarine in a Realistic Surfaced Sea State Condition for Predictions of Hydrodynamic Wave Impact Loading", Proceedings of the ASME 30th International Conference on Offshore Mechanics and Arctic Engineering Rotterdam, Netherlands, June l9-24, 2011.

[5] Jiang, M., Lien, V., Lesar, D., Engle, A. and R. Lewis. “A Validation of Various Codes Using Hydrodynamic Wedge Impact Data,” Proceedings of the ASME 31th International Conference on Offshore Mechanics and Arctic Engineering, June 10 - June 15, 2012, Rio de Janeiro, Brazil.

[6] Lin, W.-M., Collette, M., Lavis, D., Jessup, S., and J. Kuhn. “Recent Hydrodynamic Tool Development and Validation for Motions and Slam Loads on Ocean-Going High-Speed Vessels.” 10th International Symposium on the Practical Design of Ships and Other Floating Structures, 2007.

THIS PAGE INTENTIONALLY LEFT BLANK

APPENDIX A: CALIBRATION OF KISTLER GAUGES

The "Kistler Gauge" dynamometer was constructed using four Kistler force sensors capable of measuring force in three axes. The sensors were sandwiched between two plates of 1-inch thick heat-treated 17-4 stainless steel and preloaded as per manufacturer's specification. The voltages were recorded using a computer based data acquisition system. The gauge assembly is shown in Figure A-1.

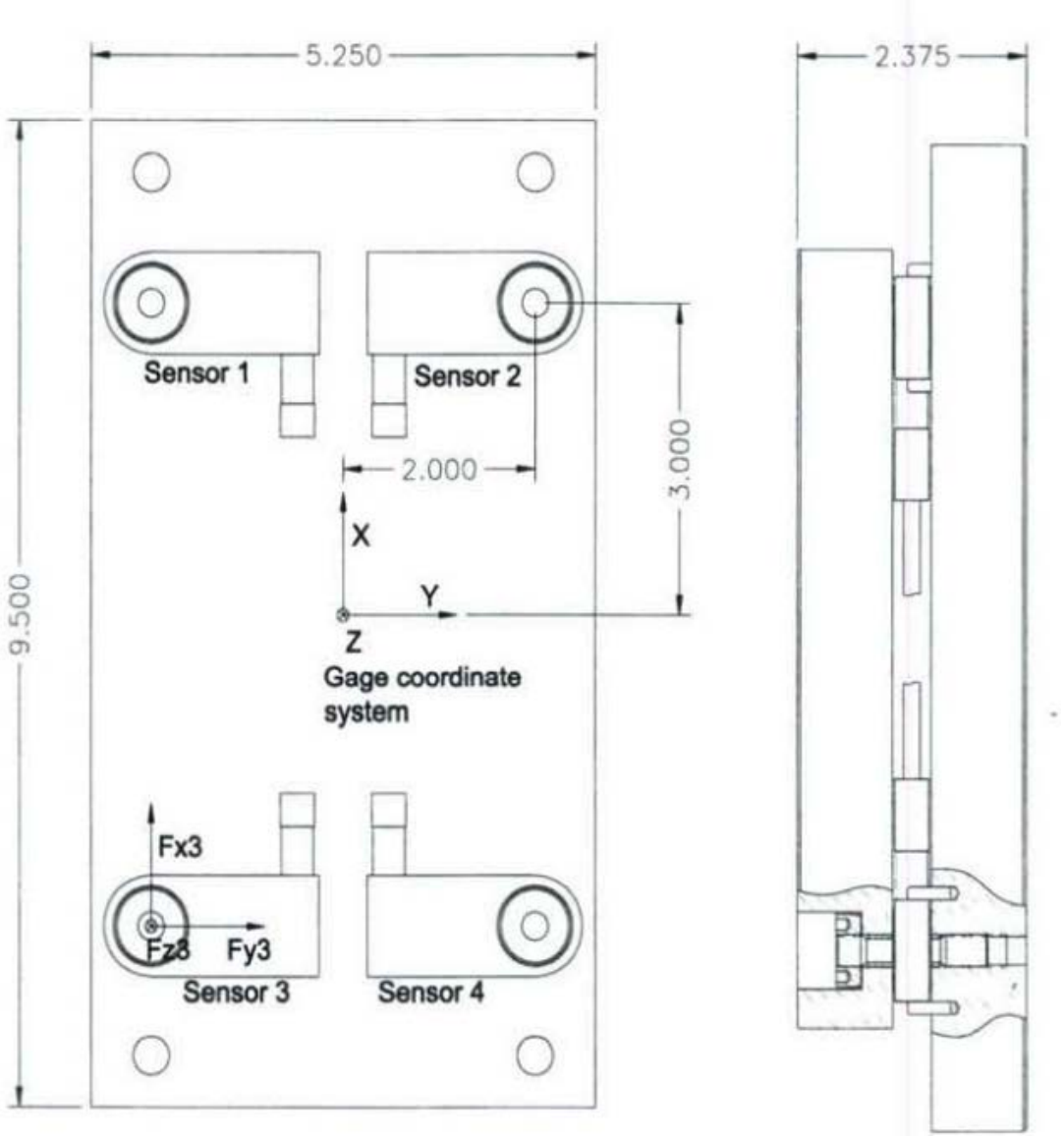

Figure A - 1. Kistler Gauge Assembly

To calibrate the dynamometer, dead weights were placed at specified load points. The input load and the output voltages were recorded for each load. Each axis was loaded in force and moment independently for approximately 140 load points. The measurements were averaged for 3 seconds at 100 Hz sample rate. The voltages were converted to engineering units using the single axis calibrations performed prior to assembly of the gauge. Since the sensor coordinate system did not always align with the gauge coordinate system the forces from the sensors were rotated into the gauge coordinate system. The forces and moments on the gauge assembly were calculated using equations A-1 through A-6:

$$Fx_{sum} = Fx1 + Fx2 + Fx3 + Fx4 \quad \text{(A-1)}$$

$$Fy_{sum} = Fy1 + Fy2 + Fy3 + Fy4 \quad \text{(A-2)}$$

$$Fz_{sum} = Fz1 + Fz2 + Fz3 + Fz4 \quad \text{(A-3)}$$

$$Mx_{sum} = Ry * (-Fz1 + Fz2 - Fz3 + Fz4) \quad \text{(A-4)}$$

$$My_{sum} = Rx * (-Fz1 - Fz2 + Fz3 + Fz4) \quad \text{(A-5)}$$

$$Mz_{sum} = Ry * (Fx1 - Fx2 + Fx3 - Fx4) + Rx * (Fy1 + Fy2 - Fy3 - Fy4) \quad \text{(A-6)}$$

where *FxN* = force in X direction from gauge N,

FyN = force in Y direction from gauge N,

FzN = force in Z direction from gauge N,

Fx_{sum} = sum of forces in X direction,

Fy_{sum} = sum of forces in Y direction,

Fz_{sum} = sum of forces in Z direction,

Mx_{sum} = sum of moments about the X axis,

My_{sum} = sum of moments about the Y axis, and

Mz_{sum} = sum of moments about the Z axis

The input loads and the calculated forces and moments above were used to generate an interaction matrix, A^{-1}**,** using a Pseudo Inverse Technique shown in A-8.

$$F_{sum} = F * A \quad \text{(A-7)}$$

$$A^{-1} = ((F^T * F)^{-1} * F^T * F_{sum})^{-1} \quad \text{(A-8)}$$

where F_{sum} = (6 x N) matrix containing forces and moments calculated from voltages

F = (6 x N) matrix containing applied loads (forces and moments)

Equation A-9 is then used to derive an applied load given measured the measured forces:

$$F = F_{sum} * A^{-1} \quad \text{(A-9)}$$

The error of the measurements was calculated using A-10:

$$Error = F - F_{sum} \quad \text{(A-10)}$$

Table A-1 and Table A-2 below summarize the calibration results of each gague used during testing. The “max” and “min” values represent the maximum and minimum errors over the whole range of the calibration. The largest error in force for the forward gauge (2002-3), at the tow post, was 0.42% and in moment, it was 0.16%. For the aft gauge (2002-4), at the grasshopper, the largest error in force was 0.50% and in moment, it was 0.20%.

Table A- 1. Forward Kistler Gauge Calibration Error Report

Kistler Gauge 2003-3 (Forward)						
	FX	***FY***	***FZ***	***MX***	***MY***	***MZ***
	(LBS)	***(LBS)***	***(LBS)***	***(FT-LB)***	***(FT-LB)***	***(FT-LB)***
RANGE	***100***	***100***	***650***	***122.9167***	***122.9167***	***50.78125***
	FX	***FY***	***FZ***	***MX***	***MY***	***MZ***
% ERROR	***(%)***	***(%)***	***(%)***	***(%)***	***(%)***	***(%)***
	0.14	***0.11***	***0.10***	***0.14***	***0.15***	***0.30***
	-0.32	***-0.42***	***-0.17***	***-0.08***	***-0.14***	***-1.16***
	FX	***FY***	***FZ***	***MX***	***MY***	***MZ***
ERROR	***(LBS)***	***(LBS)***	***(LBS)***	***(FT-LB)***	***(FT-LB)***	***(FT-LB)***
MAX	0.14	0.11	0.62	0.18	0.19	0.15
MIN	-0.32	-0.42	-1.11	-0.10	-0.17	-0.59
STDEV	0.07	0.08	0.26	0.03	0.05	0.15

Table A- 2. Aft Kistler Gauge Calibration Error Report

Kistler Gauge 2003-4 (Aft)						
	FX	***FY***	***FZ***	***MX***	***MY***	***MZ***
	(LBS)	***(LBS)***	***(LBS)***	***(FT-LB)***	***(FT-LB)***	***(FT-LB)***
RANGE	**100**	**100**	**650**	**122.9167**	**122.9167**	**50.78125**
	FX	***FY***	***FZ***	***MX***	***MY***	***MZ***
% ERROR	***(%)***	***(%)***	***(%)***	***(%)***	***(%)***	***(%)***
	0.20	**0.17**	**0.12**	**0.11**	**0.14**	**0.18**
	-0.31	**-0.50**	**-0.14**	**-0.14**	**-0.20**	**-0.12**
	FX	***FY***	***FZ***	***MX***	***MY***	***MZ***
ERROR	***(LBS)***	***(LBS)***	***(LBS)***	***(FT-LB)***	***(FT-LB)***	***(FT-LB)***
MAX	0.20	0.17	0.80	0.14	0.17	0.09
MIN	-0.31	-0.50	-0.89	-0.18	-0.24	-0.06
STDEV	0.12	0.15	0.32	0.05	0.08	0.03

THIS PAGE INTENTIONALLY LEFT BLANK

APPENDIX B: SWINGING PROCEDURE

The inertial frame used to swing the model consists of an “A-frame” type steel horse approximately 12 feet high, 8.4 feet long, and 8 feet wide. A stainless steel pivot post comes down from the steel structure and is used to support the model in a pendulum type fashion. The pivot post works in conjunction with a vertical pivot point and associated pivot hardware such that a model up to 1200 pounds, 22 feet long, and 6 feet wide can be swung under the inertial frame. The “A-frame” pivot post and the associated pivot support attachments for both the post and the model can be rotated. In this way, the model can be swung about both the roll and pitch axes without having to rotate the model in yaw or re-attaching the model pivot hardware. For this test, the model was dynamically ballasted for pitch so no roll ballast was performed other than ensuring that the model would have a static heel angle of zero.

The model longitudinal center of gravity (LCG) was defined as 97.4 inches forward of the transom. The tow pivot hardware and the ballast pivot hardware were located and attached this LCG. When performing a dynamic ballast of the model for displacement mode, the effective LCG is assumed to be the same as the static LCG and all pitch ballast procedures are performed about this LCG. To ballast the model for pitch, the model is weighed prior to attachment and then additional ballast weight is added to match the design test weight, less any point load exerted by the heave post and towing hardware. Ballast weights are shifted forward, aft, port, and starboard to zero the model in roll and pitch. The model vertical center of gravity (VCG) is then determined on the A-frame by moving an inclining weight along the longitudinal axis and measuring the change in trim angle due to the corresponding moment of the inclining weight. From these values, the model VCG can be determined relative to the A-frame pivot, which in turn can be defined relative to the model. This procedure is performed over a range of several small angles of inclination to ensure accuracy and repeatability.

The pitch moment of inertia is determined by swinging the model about the pitch axis at small angles and measuring the pitch period. Using pendulum equations, the pitch moment of inertia about the “A-frame” pivot point can be calculated. The inertia due to the “A-frame” attachment pivot can then be subtracted, and the inertia due to the heave and pitch tow bracket can be included to determine the final model pitch moment of inertia. The calculated pitch moment of inertia about the “A-frame” pivot is translated to a model reference using the parallel axis theorem. Any other known model components can be included in the final model weight, center of gravity, or gyradius efforts by appropriate calculations. Ultimately, all physical properties should be translated and represented relative to the model coordinates.

THIS PAGE INTENTIONALLY LEFT BLANK

APPENDIX C: SAMPLE BALLAST PLAN

Below is a sample ballast spreadsheet for a post-test measurement of model mass properties, including LCG, VCG, and pitch gyradius for the *Athena* Model 5365. These measurements were made before and after the test to account for any weight that may had been intentionally or unintentionally shifted during the course of testing.

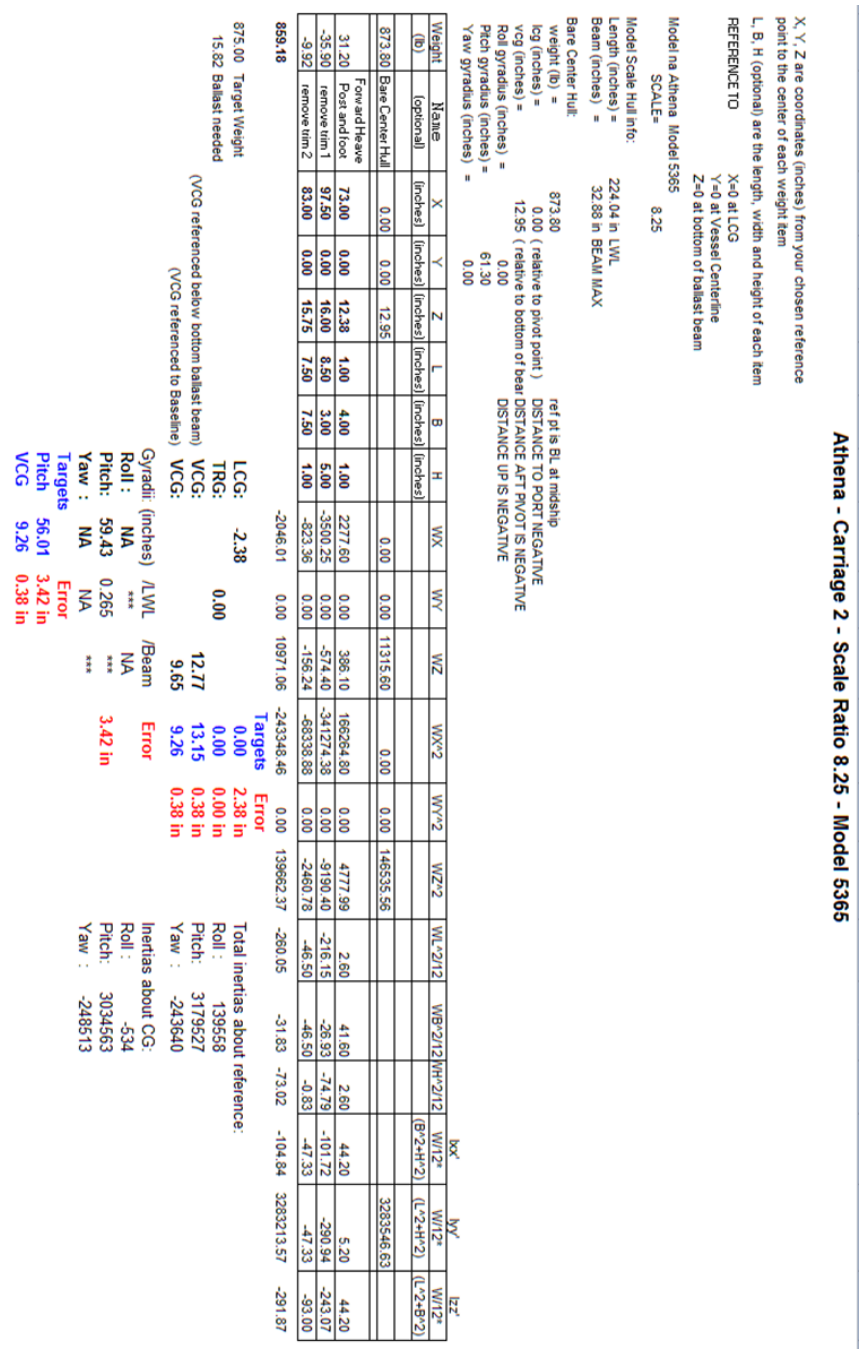

Athena - Carriage 2 - Scale Ratio 8.25 - Model 5365

X, Y, Z are coordinates (inches) from your chosen reference point to the center of each weight item

L, B, H (optional) are the length, width and height of each item

REFERENCE TO X=0 at LCG
Y=0 at Vessel Centerline
Z=0 at bottom of ballast beam

Model na Athena Model 5365
SCALE= 8.25

Model Scale Hull info:
Length (inches) = 224.04 in LWL
Beam (inches) = 32.88 in BEAM MAX

Bare Center Hull:
weight (lb) = 873.80 ref pt is BL at midship
lcg (inches) = 0.00 (relative to pivot point) DISTANCE TO PORT NEGATIVE
vcg (inches) = 12.95 (relative to bottom of bear DISTANCE AFT PIVOT IS NEGATIVE
Roll gyradius (inches) = 0.00 DISTANCE UP IS NEGATIVE
Pitch gyradius (inches) = 61.30
Yaw gyradius (inches) = 0.00

Weight (lb)	Name (optional)	X (inches)	Y (inches)	Z (inches)	L (inches)	B (inches)	H (inches)	WX	WY	WZ	WX^2	WY^2	WZ^2	WL^2/12	WB^2/12	WH^2/12	box' Wl/12* (B^2+H^2)	hy' Wl/12* (L^2+H^2)	bz' Wl/12* (L^2+B^2)
873.80	Bare Center Hull	0.00	0.00	12.95				0.00	0.00	11315.60	0.00	0.00	146535.56						3283546.63
31.20	Fore and Heave Post and foot	73.00	0.00	12.38	1.00	4.00	1.00	2277.60	0.00	386.10	166264.80	0.00	4777.99	2.60	41.60	2.60	44.20	5.20	44.20
-35.90	remove tim 1	97.50	0.00	16.00	8.50	3.00	5.00	-3500.25	0.00	-574.40	-341274.38	0.00	-9190.40	-216.15	-26.93	-74.79	-101.72	-290.94	-243.07
-9.92	remove tim 2	83.00	0.00	15.75	7.50	7.50	1.00	-823.36	0.00	-156.24	-68338.88	0.00	-2460.78	-46.50	-46.50	-0.83	-47.33	-47.33	-93.00
859.18								-2046.01	0.00	10971.06	-243348.46	0.00	139682.37	-260.05	-31.83	-73.02	-104.84	3283213.57	-291.87

(VCG referenced below bottom ballast beam) (VCG referenced to Baseline)

875.00 Target Weight
15.82 Ballast needed

LCG: -2.38
TRG:
VCG: 0.00

	Targets	Error
	0.00	2.38 in
	0.00	0.00 in
	13.15	0.38 in
	9.26	0.38 in

Gyradii: (inches) /LWL /Beam Error
Roll : NA *** NA
Pitch: 59.43 0.265 *** 3.42 in
Yaw : NA NA ***

Targets Error
Pitch 56.01 3.42 in
VCG 9.26 0.38 in

Total inertias about reference:
Roll : 139558
Pitch: 3179527
Yaw : -243640

Inertias about CG:
Roll : -534
Pitch: 3034563
Yaw : -248513

THIS PAGE INTENTIONALLY LEFT BLANK

APPENDIX D: *ATHENA* CALM WATER MODEL TEST – UNCERTAINTY ANALYSIS

BACKGROUND

A detailed uncertainty analysis of the calm water *Athena* model data was performed, using the approach outlined in Coleman and Steele [D-1], Chapter 4 and Appendix B. This approach includes the standards issued by the American Society of Mechanical Engineers (ASME) [D-2], revision of [D-3] and the American Institute of Aeronautics and Astronautics (AIAA) [D-4]. This approach adopts the methodology of the ISO Guide [D-5], though the terminology differs, specifically in the categorization of the uncertainties.

Figure D - 1 (Coleman and Steele [D-1]) shows a flow diagram of the propagation of errors into the experimental results. The individual measurement systems (1, 2,…J) used in the experiment are influenced by a number of elemental error sources. The elemental errors are made up of a bias, or systematic, (B_1, B_2,…, BJ) error and a precision, or random, (P_1, P_2,…, PJ) error in the measured value of the variable. The bias error is the fixed or constant component of the total error and is referred to as systematic error. The precision (or random) error quantifies the repeatability of the measurement. These errors then propagate through the data reduction equation ($r=r(X_1, X_2,…X_J)$) and result in a bias (B_r) and precision (P_r) error in the final experimental result.

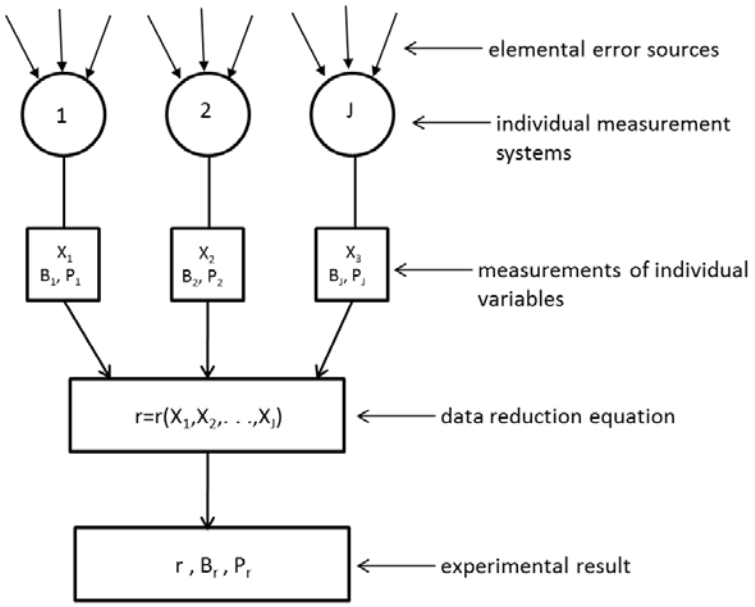

Figure D - 1. Propagation of Errors into an Experimental Result [D-1]

The general data reduction equation is shown in Equation (D-1), where r is the experimental result determined from J measured variables, X_i:

$$r = r(X_1,X_2,\ldots,X_J) \tag{D-1}$$

The total uncertainty is given by:

$$U_r^2 = B_r^2 + P_r^2 \tag{D-2}$$

where U_r = overall uncertainty, B_r = bias uncertainty and P_r = precision uncertainty.

The bias uncertainty is defined as:

$$B_r^2 = \sum_{i=1}^{J} \theta^2 B_i^2 + 2\sum_{i=1}^{J-1}\sum_{k=i+1}^{J} \theta_i\theta_j B_{ik} \tag{D-3}$$

where B_i = bias uncertainty of the measured variables X_i in Equation (D-1), and B_{ik} is the covariance estimator for the systematic errors in X_i and X_k defined as:

$$B_{ik} = \sum_{\alpha=1}^{L} (B_i)_\alpha (B_k)_\alpha \tag{D-4}$$

where L is the number of elemental systematic error sources that are common for measurements of variables X_i and X_k, and θ_i is the sensitivity coefficient, defined as the partial derivative of r with respect to the individual variables X_i:

$$\theta_i = \frac{\partial r}{\partial X_i} \tag{D-5}$$

The precision uncertainty is (assuming no correlated precision errors):

$$P_r^2 = \sum_{i=1}^{J} \theta^2 P_i^2 \tag{D-6}$$

where P_i = precision uncertainty of the variables X_i in Equation (D-1). This equation assumes that the instrument uncertainties are independent.

The first step of the uncertainty analysis is to estimate the biases due to elemental errors that affect the individual measurement systems. These biases can include (but are not limited to) calibration errors, data acquisition errors, and conceptual errors. There is no way to calculate bias errors directly; they must always be estimated [D-1]. The approach described here assumes that they are estimated at the 95% confidence interval. The total bias error for each measurement system is the root-sum-square (*RSS*) of the individual bias uncertainties for each variable X_i:

$$B_j = \left[\sum_{k=1}^{M} (B_j)_k^2\right]^{1/2} \tag{D-7}$$

Once the bias uncertainties are estimated for each of the measured variables, the total bias (systematic) uncertainty can be determined from Equation (D-3). In cases where the different variables do not share common elemental error sources, the covariance terms are zero, and Equation (D-3) becomes:

$$B_r^2 = \left(\frac{\partial r}{\partial X_1}\right)^2 B_1^2 + \left(\frac{\partial r}{\partial X_2}\right)^2 B_2^2 + \cdots + \left(\frac{\partial r}{\partial X_J}\right)^2 B_J^2 \tag{D-8}$$

or:

$$B_r^2 = (\theta_1)^2 B_1^2 + (\theta_2)^2 B_2^2 + \cdots + (\theta_J)^2 B_J^2 \tag{D-9}$$

The calculation of the precision (random) uncertainty is shown in Equation (D-6), which is the *RSS* of the precision limits for the individual variables multiplied by their sensitivity coefficients. Precision uncertainties are assumed to have a Gaussian distribution, which "has been found to describe more real cases of experimental and instrument variability than any other distribution" [D-1]. The standard deviation of the parent population is unknown, so the sample standard deviation of the average result, $\bar{x}$, from N tests must be used instead:

$$S_x = \left[\frac{1}{N-1}\sum_{i=1}^{N} (X_i - \bar{X})^2\right]^{1/2} \tag{D-10}$$

Equation (D-10) applies in the case of one test with N samples. If instead there M = 10 sets of readings, and an average value is calculated for each of the 10 sets, the standard deviation of the

means is of interest. This approach is typical for this application, where multiple runs are made under the same conditions to evaluate repeatability. In this case, the sample means are normally distributed with mean μ and standard deviation:

$$\sigma_{\bar{x}} = \frac{\sigma}{\sqrt{M}} \tag{D-11}$$

Again, the standard deviation of the parent population is unknown, so the sample standard deviation must be used, with S_x defined as in Equation (D-10):

$$S_{\bar{x}} = \frac{S_x}{\sqrt{M}} \tag{D-12}$$

The next step is to estimate the precision uncertainty at a 95% confidence interval. For a Gaussian distribution with mean μ and parent population standard deviation of σ:

$$Prob(X_i - 1.96\sigma \leq \mu \leq X_i + 1.96\sigma) = 0.95 \tag{D-13}$$

which states with 95% confidence the mean of the parent distribution is within +/-1.96σ of a single reading from that distribution. For averages calculated from *M* sets of *N* readings, this becomes:

$$Prob\left(\bar{X} - 1.96\frac{\sigma}{\sqrt{M}} \leq \mu \leq \bar{X} + 1.96\frac{\sigma}{\sqrt{M}}\right) = 0.95 \tag{D-14}$$

Again, σ is unknown, and the sample standard deviation must be used instead which yields:

$$Prob\left(-t \leq \frac{X - \mu}{S_x} \leq t\right) = 0.95 \tag{D-15}$$

and

$$Prob\left(-t \leq \frac{\bar{X} - \mu}{S_x/\sqrt{M}} \leq t\right) = 0.95 \tag{D-16}$$

where *t* is no longer equal to 1.96 (as in Eq. 13) because S_x is based on a finite number of readings. The variables $\frac{\bar{X}-\mu}{S_x}$ and $\frac{\bar{X}-\mu}{S_x/\sqrt{M}}$ are not normally distributed [D-1]. These variables instead follow the *t* distribution with *N*-1 or *M*-1 degrees of freedom, respectively. A table of values for *t* can be found in Table A.2 of Appendix A of [D-1].

From this, with a 95% confidence limit for a sample of *N* measurements of *X* drawn from a Gaussian distribution, the precision uncertainty of the mean result is:

$$P_{\overline{X_i}} = tS_{\overline{X_i}} \tag{D-17}$$

where t=coverage factor based on the degrees of freedom, found in Table A.2, Appendix A [1].

For $M \geq 10$, a coverage factor of two is advised. If $M < 10$, a coverage factor of two is still acceptable if the bias and precision uncertainties are of similar magnitude. Coleman and Steele advise that the large sample equations (i.e. $t = 2$) are applicable in the vast majority of engineering testing ([D-1], p. 85).

The precision uncertainties for each variable are then propagated through Eq. (D-6), and the total uncertainty for the experimental result is:

$$U_r^2 = B_r^2 + P_r^2 \tag{D-18}$$

where $r \pm U_r$ provides a 95% confidence interval for the true result. With alternate approaches (e.g. ISO), the bias and precision uncertainties are combined before expanding to 95% confidence intervals. This approach assumes the combined error distributions are Gaussian, even if the individual uncertainties are not. This approach also requires an estimate to approximate the effective degrees of freedom using the Welch-Satterthwaite formula.

As an alternative to the precision uncertainty process described above, in the type of experimental program where multiple tests are performed using the same experimental apparatus and the final experimental result is determined as the mean of the results of the individual tests, the precision uncertainty can be determined directly. In an experiment where a single test is replicated *M* times, resulting in individual values $r_1, r_2, \ldots, r_M$ for the data reduction equation in Equation (D-1), and the values are averaged to produce the "best" result:

$$\bar{r} = \frac{1}{M}\sum_{k=1}^{M} r_k \tag{D-19}$$

The bias uncertainty for this test is the same as for a single test, and is still determined according to the method described above. Biases are fixed errors, and are not affected by averaging the results of multiple tests.

The standard deviation of the results from the *M* individual tests (with *M*-1 degrees of freedom) is given by:

$$S_r = \left[\frac{1}{M-1}\sum_{k=1}^{M}(r_k - \bar{r})^2\right]^{1/2} \tag{D-20}$$

The standard deviation of the average result is then:

$$S_{\bar{r}} = \frac{S_r}{\sqrt{M}} \tag{D-21}$$

And the overall precision uncertainty for the computed variable, *r* is:

$$P_{\bar{r}} = tS_{\bar{r}} \tag{D-22}$$

The total uncertainty is then the same as Eq. (18):

$$U_{\bar{r}}^2 = B_r^2 + P_{\bar{r}}^2 \tag{D-23}$$

In this method, the overall precision uncertainty is computed directly, instead of being calculated for individual inputs and propagated through the data reduction equation (DRE). Coleman and Steele advise that when multiple readings of all the variables can be obtained over an appropriate time period, the direct determination method for P_r is advantageous due to the possibility that the random errors in different variables are correlated (p. 105).

APPROACH

Total Resistance

The data reduction equation for total resistance (R_t) for the calm water *Athena* model data is:

$$R_t = F_{xfwd} + F_{xaft}\cos(\tau) + F_{zaft}\sin(\tau) \tag{D-24}$$

where F_{xfwd} = resistance measured at forward Kistler gauge, located under the tow post
F_{xaft} = resistance measured at aft Kistler gauge, located under the grasshopper
τ = trim angle

The forward Kistler gauge is located above the model pivot point, so the direction is earth-fixed. The aft Kistler gauge is mounted to the model, so it needs to be corrected to earth-fixed resistance in the x-direction.

The total uncertainty for R_t is:

$$U_{\overline{R_t}}^2 = B_{R_t}^2 + P_{\overline{R_t}}^2 \tag{D-25}$$

The total bias uncertainty is:

$$B_{R_t}^2 = B_{F_{xfwd}}^2\theta_{F_{xfwd}}^2 + B_{F_{xaft}}^2\theta_{F_{xaft}}^2 + B_{F_{zaft}}^2\theta_{F_{zaft}}^2 + B_\tau^2\theta_\tau^2 \tag{D-26}$$

where the sensitivity coefficients for each variable are as follows:

$$\theta_{F_{xfwd}} = \frac{\partial R_T}{\partial F_{xfwd}} = 1 \tag{D-27}$$

$$\theta_{F_{xaft}} = \frac{\partial R_T}{\partial F_{xaft}} = \cos(\tau) \tag{D-28}$$

$$\theta_{F_{yaft}} = \frac{\partial R_T}{\partial F_{yaft}} = \sin(\tau) \tag{D-29}$$

$$\theta_\tau = \frac{\partial R_T}{\partial \tau} = -F_{xaft}\sin(\tau) + F_{zaft}\cos(\tau) \tag{D-30}$$

An additional error in the resistance measurement may result from a slight off angle during installation (τ). This error would cause the difference in the force between measured and actual to be:

$$\Delta F = F_{xmeas} - F_{xmeas}\cos\alpha \tag{D-31}$$

which makes the bias due to an off angle installation (for each gauge individually):

$$B_\alpha^2 = B_{F_{xmeas}}^2\theta_{F_{xmeas}}^2 + B_\alpha^2\theta_\alpha^2 \tag{D-32}$$

where the sensitivity coefficients are:

$$\theta_{F_{xmeas}} = 1 - \cos\alpha \tag{D-33}$$

$$\theta_\alpha = -F_{xmeas}\sin\alpha \tag{D-34}$$

For small angles of 0.5 degrees or less (which is the resolution of the inclinometer used), both Eqs. D-33 and D-34 become zero, so these errors will be ignored.

Bias uncertainty for *Fx* and *Fy* at the forward and aft position include the calibration errors for the Kistler gauges and the errors in the weights used for the calibration. The bias errors are listed in Table D - 1. The second column in the table shows either the standard deviation of the

instrument (S, from calibration, etc.) or the reported range (see "Notes" column for detail). If the standard deviation is given, the errors are assumed to be Gaussian and multiplied by 2 to yield the 95% confidence intervals. If the range is given, the errors are assumed uniform and divided by the square root of three [D-5] (Section 4.3.7).

Table D - 1. Uncertainties for Resistance Measurement

Description	*S* or Range	*N*	*B* lbs	Notes
Kistler 2003-3 Fx (fwd)	0.07 lbs	154	0.14	calibration error, Gaussian
Kistler 2003-3 Fy (fwd)	0.08 lbs	154	0.16	calibration error, Gaussian
Kistler 2003-4 Fx (aft)	0.12 lbs	164	0.24	calibration error, Gaussian
Kistler 2003-4 Fy (aft)	0.15 lbs	164	0.30	calibration error, Gaussian
Calibration weights	+/-0.1	n/a	0.06	estimated by test engineer, rectangular

**B* is estimated at 95% confidence interval

Trim

The data reduction equation for the trim angle from the initial condition:

$$\tau = \text{asin}\left(\frac{\sigma_{FSP} - \sigma_{ASP}}{L_{SP}}\right) \tag{D-35}$$

where σ_{FSP} = sinkage at forward string potentiometer
σ_{ASP} = sinkage at aft string potentiometer
L_{FSP} = distance between string potentiometers

The total uncertainty for τ is:

$$U_\tau^2 = B_\tau^2 + P_{\bar{\tau}}^2 \tag{D-36}$$

The total bias uncertainty is:

$$B_\tau^2 = B_{\sigma_{FSP}}^2\theta_{\sigma_{FSP}}^2 + B_{\sigma_{ASP}}^2\theta_{\sigma_{ASP}}^2 + B_{L_{SP}}^2\theta_{L_{SP}}^2 \tag{D-37}$$

where the sensitivity coefficients for each variable are as follows:

$$\theta_{\sigma_{FSP}} = \frac{\partial\tau}{\partial\sigma_{FSP}} = \frac{1}{L_{SP}\sqrt{1 - \left(\frac{\sigma_{FSP} - \sigma_{ASP}}{L_{SP}}\right)^2}} \tag{D-38}$$

$$\theta_{\sigma_{ASP}} = \frac{\partial \tau}{\partial \sigma_{ASP}} = \frac{1}{-L_{SP}\sqrt{1-\left(\frac{\sigma_{FSP}-\sigma_{ASP}}{L_{SP}}\right)^2}} \tag{D-39}$$

$$\theta_{\sigma_{FSP}} = \frac{\partial \tau}{\partial L_{SP}} = \frac{\sigma_{FSP}-\sigma_{ASP}}{-L_{SP}^2\sqrt{1-\left(\frac{\sigma_{FSP}-\sigma_{ASP}}{L_{SP}}\right)^2}} \tag{D-40}$$

Bias uncertainties for the trim calculation include the calibration errors for the string potentiometers and error in measuring the distance between the sensors. These bias errors are listed in Table D - 2.

Table D - 2. Uncertainties for Trim Measurement

Description	S or Range	N	B	Notes
Fwd string pot	0.02 in	33	0.04 in	standard error of regression, Gaussian
Aft string pot	0.03 in	33	0.06 in	standard error of regression, Gaussian
Length between pots	+/- 1/16 inch	n/a	0.04 in	estimated by test engineer, rectangular

*B is estimated at 95% confidence interval

Sinkage

The data reduction equation for the sinkage at LTP (σ_{LTP}) from the initial condition is:

$$\sigma_{LCG} = \sigma_{ASP} + X_{TP}\left(\frac{\sigma_{FSP} - \sigma_{ASP}}{L_{SP}}\right) \tag{D-41}$$

where σ_{FSP} = sinkage at forward string potentiometer
σ_{ASP} = sinkage of aft string potentiometer
L_{FSP} = distance between string potentiometers
X_{TP} = x position of tow point (measured along the model from aft potentiometer)

The total uncertainty for σ is:

$$U_{\bar{\sigma}}^2 = B_{\sigma}^2 + P_{\bar{\sigma}}^2 \tag{D-42}$$

The total bias uncertainty is:

$$B_{\sigma}^2 = B_{\sigma_{FSP}}^2\theta_{\sigma_{FSP}}^2 + B_{\sigma_{ASP}}^2\theta_{\sigma_{ASP}}^2 + B_{L_{SP}}^2\theta_{L_{SP}}^2 \tag{D-43}$$

where the sensitivity coefficients for each variable are as follows:

$$\theta_{\sigma_{FSP}} = \frac{\partial\sigma_{TP}}{\partial\sigma_{FSP}} = \frac{X_{TP}}{L_{SP}} \tag{D-44}$$

$$\theta_{\sigma_{ASP}} = \frac{\partial\sigma_{TP}}{\partial\sigma_{ASP}} = 1 - \frac{X_{TP}}{L_{SP}} \tag{D-45}$$

$$\theta_{L_{FSP}} = \frac{\partial\sigma_{TP}}{\partial L_{SP}} = -\frac{X_{TP}(\sigma_{FSP} - \sigma_{ASP})}{L_{SP}^2} \tag{D-46}$$

Bias uncertainties for the sinkage calculation include the calibration errors for the string potentiometers, error in measuring the distance between the sensors, and the uncertainty in the LTP measurement. These bias errors are listed in Table D - 3.

Table D - 3. Uncertainties for Sinkage Measurement

Description	*S* or Range	*N*	B	Notes
Fwd string pot	0.02 in	33	0.04 in	standard error of regression, Gaussian
Aft string pot	0.03 in	33	0.06 in	standard error of regression, Gaussian
Length between pots	+/- 1/16 inch	n/a	0.04 in	estimated by test engineer, rectangular
LCG	n/a	n/a	0.1 in	see description below

**B* is estimated at 95% confidence interval

Mass Properties

Table D - 4 shows the uncertainties used to calculate model mass properties.

Table D - 4. Uncertainties for Instrumentation in Calculation of Model Mass Properties

Description	*S* or Range	*B*	Notes
trim/add'l weights	0.1 lb	0.06 lb	estimated by test engineer, rectangular
location	0.0625 in	0.0361 in	estimated by test engineer, rectangular
model weight	0.5 lb	0.3 lb	estimated by test engineer, rectangular
overall trim angle	0.5º	0.3º	includes uncertainty from determining BL
relative trim angle for VCG	n/a	0.055º	Wyler inclinometer

**B* is estimated at 95% confidence interval

Weight/Displacement

The weight of the model is given by the summation of the weights, as shown in Eq. 49:

$$W_M = \sum_{i=1}^{n} W_i \tag{D-47}$$

where W_m is the total weight of the model, and W_i are the individual components.

Since the partial derivative of Eq. 49 with respect to the individual weights is one, the bias uncertainty for weight becomes the sum of the individual weight bias uncertainties:

$$B_M^2 = \sum_{i=1}^{n} B_i^2 \tag{D-48}$$

Table D - 5 shows the bias uncertainties for the individual components of the bias uncertainty for weight, as well as the resultant overall model uncertainty. The uncertainty the model weight is the dominating factor.

Table D - 5. Uncertainty in Overall Weight

Description	*S* or Range	*B*
	(lb)	(lb)
hull/instrumentation	0.50	0.29
heave post	0.10	0.06
trim weight 1	0.10	0.06
trim weight 2	0.10	0.06
overall		0.3

**B* is estimated at 95% confidence interval

Longitudinal Center of Gravity (LCG)

The longitudinal center of gravity of the model was determined by suspending the model and a beam beneath an A-frame, attached with a pivot (a detailed description is found in Appendix B). The model is leveled by adding trim weights; trim angle is measured with an inclinometer. Once the model is level, the LCG location is under the pivot point. The trim weights are then removed computationally to determine the final LCG. The equation to calculate LCG is given by:

$$x_m = \sum_{i=1}^{n} x_i \frac{W_i}{W_M} \tag{D-49}$$

where x_i is the location of the individual weights.

The total bias uncertainty due to the model weight, trim weights and other additional weights is then:

$$B_{LCG_W}^2 = B_{W_i}^2 \theta_{W_i}^2 + B_{x_i}^2 \theta_{x_i}^2 + B_{W_M}^2 \theta_{W_M}^2 \tag{D-50}$$

where the sensitivity coefficients are:

$$\theta_{W_i} = \sum_{i=1}^{n} \frac{x_i}{W_M} \tag{D-51}$$

$$\theta_{x_i} = \sum_{i=1}^{n} \frac{W_i}{W_M} \tag{D-52}$$

$$\theta_{W_m} = \sum_{i=1}^{n} \frac{-x_i W_i}{W_M^2} \tag{D-53}$$

One other contributor to the uncertainty in LCG is the uncertainty in the trim angle measurement. If it is slightly off level, there will be a deviation for LCG. The deviation is given by:

$$\tan \emptyset = \frac{x}{z} \tag{D-54}$$

For small angles, this becomes:

$$\emptyset = \frac{x}{z} \tag{D-55}$$

where $\emptyset$ = pitch angle, x is the deviation from LCG, and z is the vertical distance from the pivot point to the CG (calculation of vertical center of gravity is described below). Defining it in terms of deviation from LCG becomes:

$$x = \emptyset z \tag{D-56}$$

The bias uncertainty due to model levelness is:

$$B_{LCG_\emptyset}^2 = B_\emptyset^2 \, \theta_\emptyset^2 + B_z^2 \theta_z^2 \tag{D-57}$$

where the sensitivity coefficients are:

$$\theta_\emptyset = z \tag{D-58}$$

$$\theta_z = \emptyset \tag{D-59}$$

For small angles, Eq. D-61 is near zero, and the overall uncertainty for LCG is:

$$B_{LCG}^2 = B_{W_i}^2 \theta_{W_i}^2 + B_{x_i}^2 \theta_{x_i}^2 + B_{W_M}^2 \theta_{W_M}^2 + B_\emptyset^2 \, \theta_\emptyset^2 \tag{D-60}$$

Table D - 6. Overall Uncertainty for LCG

Description	
$B_{W_i}^2 \theta_{W_i}^2$	0.008 in^2
$B_{x_i}^2 \theta_{x_i}^2$	0.000 in^2
$B_{W_M}^2 \theta_{W_M}^2$	0.000 in^2
$B_{\emptyset}^2 \theta_{\emptyset}^2$	0.011 in^2
B_{LCG}	0.1 in

*B is estimated at 95% confidence interval

Vertical Center of Gravity (VCG)

The vertical center of gravity was determined by adding known weights at known distances to the model, and measuring the resulting inclination with an inclinometer. The model was inclined in trim. The equation that describes VCG of the beam and model relative to the pivot point is:

$$z = \left(\frac{w}{W_m}\right)\left(\frac{x_w}{\tan\tau} - z_w\right) \tag{D-61}$$

where w is the added weight, x_w is the longitudinal location of the added weight, z_w is the vertical location of the added weight, and τ is the trim angle induced by the weight. The sensitivity coefficients are then:

$$\theta_w = \left(\frac{1}{W_m}\right)\left(\frac{x_w}{\tan\tau} - z_w\right) \tag{D-62}$$

$$\theta_{W_m} = \left(\frac{-w}{W_m^2}\right)\left(\frac{x_w}{\tan\theta} - z_w\right) \tag{D-63}$$

$$\theta_{X_w} = \frac{w}{W_m \tan\tau} \tag{D-64}$$

$$\theta_\tau = \frac{-w x_w}{W_m \sin^2\tau} \tag{D-65}$$

$$\theta_{z_w} = \frac{-w}{W_m} \tag{D-66}$$

The uncertainty for z is then given by:

$$B_z^2 = B_W^2 \theta_W^2 + B_{W_M}^2 \theta_{W_M}^2 + B_{x_w}^2 \theta_{x_w}^2 + B_\tau^2 \theta_\tau^2 + B_{z_w}^2 \theta_{z_w}^2 \tag{D-67}$$

The *z* value for the beam alone is calculated in a similar manner. The measurement is repeated multiple times, using the average result. The uncertainty for the hull and beam VCG are shown in Table D-7, and the uncertainty estimates for the beam alone are shown in Table D - 8.

Table D - 7. Uncertainty for Model and Beam z

Description	
$B_w^2\,\theta_w^2$	0.0113 in^2
$B_{W_M}^2\theta_{W_M}^2$	0.0000 in^2
$B_{x_w}^2\,\theta_{x_w}^2$	0.0001 in^2
$B_\tau^2\,\theta_\tau^2$	0.0020 in^2
$B_{z_w}^2\theta_{z_w}^2$	0.0000 in^2
B_{zBH}	0.1 in
P_{zBH}	0.5 in
U_{zBH}	0.5 in

Table D - 8. Uncertainty for Beam z

Description	
$B_w^2\,\theta_w^2$	0.0000 in^2
$B_{W_M}^2\theta_{W_M}^2$	0.0003 in^2
$B_{x_w}^2\,\theta_{x_w}^2$	0.0000 in^2
$B_\tau^2\,\theta_\tau^2$	0.0002 in^2
$B_{z_w}^2\theta_{z_w}^2$	0.0000 in^2
B_{zB}	0.02 in
P_{zB}	0.30 in
U_{zB}	0.3 in

After *z* is calculated, the VCG of the hull alone is computed from the hull-beam combination by:

$$z_H = (W_{BH}z_{BH} - W_B z_B)/W_H \tag{D-68}$$

where W_{BH} is the weight of the hull and beam, z_{BH} is the VCG of the hull and beam (D-61), W_B is the weight of the beam, z_B is the VCG of the beam (similar to D-61) and W_H is the weight of the hull. The sensitivity coefficients for Eq. D-68 are:

$$\theta_{W_{BH}} = \frac{z_{BH}}{W_H} \tag{D-69}$$

$$\theta_{z_{BH}} = \frac{W_{BH}}{W_H} \tag{D-70}$$

$$\theta_{W_B} = \frac{-z_B}{W_H} \tag{D-71}$$

$$\theta_{z_B} = \frac{-W_B}{W_H} \tag{D-72}$$

$$\theta_{W_H} = \frac{(W_{BH} z_{BH} - W_B z_B)}{W_H^{\,2}} \tag{D-73}$$

The uncertainty for the z_H is then given by:

$$B_{z_H}^2 = B_{W_{BH}}^2 \theta_{W_{BH}}^2 + B_{z_{BH}}^2 \theta_{z_{BH}}^2 + B_{W_B}^2 \theta_{W_B}^2 + B_{z_B}^2 \theta_{z_B}^2 + B_{W_H}^2 \theta \tag{D-74}$$

Table D - 9. Uncertainty for z_H

Description	
$B_{W_{BH}}^2 \theta_{W_{BH}}^2$	0.0000 in^2
$B_{z_{BH}}^2 \theta_{z_{BH}}^2$	0.2831 in^2
$B_{W_B}^2 \theta_{W_B}^2$	0.0000 in^2
$B_{z_B}^2 \theta_{z_B}^2$	0.0013 in^2
$B_{W_H}^2 \theta_{W_H}^2$	0.0001 in^2
B_{zH}	0.53 in

The additional uncertainty of the VCG of the additional parts that are not measured during the inclining experiment must also be included in the final uncertainty. The equation for this is similar to that of the LCG calculation, where x is replaced by z:

$$z_m = \sum_{i=1}^{n} z_i \frac{W_i}{W_M} \tag{D-75}$$

The sensitivity coefficients are the same as Eq. D-51 through D-53 (replacing x with z), with the final VCG uncertainty given as; values are given in Table D-10:

$$B_{VCG_M}^2 = B_{W_i}^2 \theta_{W_i}^2 + B_{z_i}^2 \theta_z^2 + B_{W_M}^2 \theta_{W_M}^2 \tag{D-76}$$

Table D - 10. Uncertainty for VCG Summation

Description	
$B_{W_i}^2 \theta_{W_i}^2$	0.0002 in^2
$B_{z_i}^2 \theta_{z_i}^2$	0.0000 in^2
$B_{W_M}^2 \theta_{W_M}^2$	0.0000 in^2
B_{VCG_M}	0.0158 in

The total uncertainty for VCG is the RSS of the model z uncertainty and the summation uncertainty, as shown in Table D - 11.

Table D - 11. Overall Uncertainty for VCG.

Description	
B_{VCG_M}	0.0158 in
B_{zH}	0.53 in
B_{VCG}	0.5 in

Carriage Speed

The uncertainty in the carriage speed is comprised of the precision uncertainty for each run, along with the bias uncertainty from the encoder calibration. Table D - 12 shows the bias uncertainty from the calibration.

Table D - 12. Uncertainties for LCG

Description	*S* or Range	*N*	B	Notes
calibration of encoder	1.58E-4	10	3.15E-4	standard error of regression, Gaussian

**B* is estimated at 95% confidence interval

REFERENCES

[D-1] Coleman, H. and W. G. Steele. *Experimentation and Uncertainty Analysis for Engineers*, Second Edition, John Wiley and Sons, New York, 1999.

[D-2] American National Standards Institute/American Society of Mechanical Engineers. *Test Uncertainty*, PTC 19.1-1998, ASME, New York, 1998.

[D-3] American National Standards Institute/American Society of Mechanical Engineers. *Test Uncertainty*, PTC 19.1-1985 Part 1, ASME, New York, 1986.

[D-4] American Institute of Aeronautics and Astronautics, Assessment of Wind Tunnel Data Uncertainty, AIAA Standard S-071-1995, AIAA, New York, 1995.

[D-5] International Organization for Standardization, *Guide to the Expression of Uncertainty in Measurement*, ISBN 92-67-10188-9, ISO, Geneva, 1993. [Corrected and reprinted , 1995]

Distribution

	Hard Copies	*Digital Copies*
Office of Naval Research 875 North Randolph Street Arlington, VA 22203-1995 Attn: Dr. Robert Brizzolara		1
Attn: Dr. Thomas Fu		1
		1
Defense Technical Information Center 8725 John J. Kingman Road Ft. Belvoir, VA 22060-6218		
University of Iowa Attn: Dr. Frederick Stern		1

NSWC, CARDEROCK DIVISION INTERNAL DISTRIBUTION

Code	Name	*Hard Copies*	*Digital Copies*
809	D. Intolubbe	1	1
83	Technical Data Repository	1	1
1033	TIC - SCRIBE		1
833	Anne Fullerton, Jayson Geiser, Evan Lee, Craig Merrill, Jason Morin, Sarah Punzi, Christine Schleicher, Charles Weil		1

THIS PAGE INTENTIONALLY LEFT BLANK


NAVSEA
WARFARE CENTERS
Carderock